PNNL-38040

New NDA Methods for Thorium Fuel Cycle Safeguards

Final Report

July 2025

Benjamin S McDonald
Areg Danagoulian
Ethan A Klein
Jonathan M Kulisek
Michael E Moore
Jill M Rahon
Shayaan Subzwari
Mital A Zalavadia

U.S. DEPARTMENT OF ENERGY

Prepared for the U.S. Department of Energy
under Contract DE-AC05-76RL01830

PACIFIC NORTHWEST NATIONAL LABORATORY
operated by
BATTELLE
for the
UNITED STATES DEPARTMENT OF ENERGY
under Contract DE-AC05-76RL01830

Printed in the United States of America

Available to DOE and DOE contractors from
the Office of Scientific and Technical Information,
P.O. Box 62, Oak Ridge, TN 37831-0062
www.osti.gov
ph: (865) 576-8401
fox: (865) 576-5728
email: reports@osti.gov

Available to the public from the National Technical Information Service
5301 Shawnee Rd., Alexandria, VA 22312
ph: (800) 553-NTIS (6847)
or (703) 605-6000
email: info@ntis.gov
Online ordering: http://www.ntis.gov

PNNL-38040

New NDA Methods for Thorium Fuel Cycle Safeguards

Final Report

July 2025

Benjamin S McDonald
Areg Danagoulian
Ethan A Klein
Jonathan M Kulisek
Michael E Moore
Jill M Rahon
Shayaan Subzwari
Mital A Zalavadia

Prepared for
the U.S. Department of Energy
under Contract DE-AC05-76RL01830

Pacific Northwest National Laboratory
Richland, Washington 99354

This page intentionally left blank.

Abstract

This project developed portable Neutron Resonance Transmission Analysis (pNRTA) as a new non-destructive assay (NDA) method for thorium fuel cycles safeguards and other applications where multiple isotopes must be measured when present together. pNRTA leverages epithermal neutron resonances to assay multiple safeguards-relevant isotopes (e.g., ^{233}U and ^{235}U when they are present together in a sample. Existing techniques are challenged by this task, driving the need for new active interrogation methods. With selected detectors, pNRTA works in high gamma-ray backgrounds from fission and activation products and ^{232}U progeny expected in thorium fuel cycle samples. This project leveraged a pNRTA system developed at Pacific Northwest National Laboratory (PNNL) and collaboration with the Massachusetts Institute of Technology (MIT). The system uses a commercially available deuterium-tritium (DT) neutron generator at short standoff (2 m). Key achievements in this project included: first-of-a-kind pNRTA quantitative measurements of ^{233}U oxide samples, an assessment of neutron detector technologies suitable for pNRTA in high gamma-ray background environments, experimentally demonstrating quantitative assay of samples containing ^{233}U and ^{235}U, and modeling studies showing the applicability of pNRTA to a wide range of material forms. Further, a custom algorithm was developed at MIT, which provided mean bias of 9% and relative standard deviation of 36% in assaying ^{233}U, ^{235}U, ^{238}U, and ^{232}Th content in eight measured samples. These outcomes form a solid technical basis for pNRTA as a new promising capability for international safeguards verification that is portable, non-destructive, quantitative, and isotopic specific.

This page intentionally left blank.

Summary

Pacific Northwest National Laboratory (PNNL), in collaboration with the Massachusetts Institute of Technology (MIT), led the first project to explore using portable Neutron Transmission Resonance Analysis (pNRTA) for Non-Destructive Assay (NDA) measurements in future thorium fuel cycle safeguards. This technique exploits epithermal resonance structures to quantitatively determine isotopic contents in a sample. Until recently, this method has been confined to large-scale accelerator facilities (decidedly non-portable). MIT recently pioneered the use of portable neutron sources and relatively short flight paths (2 m, Figure S 1) to create useful neutron time-of-flight (TOF) spectra. It is particularly well-suited for assaying ^{233}U, ^{235}U, ^{232}Th, and possibly other isotopes of safeguards interest when they are present together in a sample. Existing techniques are challenged to accurately assay such multi-isotope mixtures.

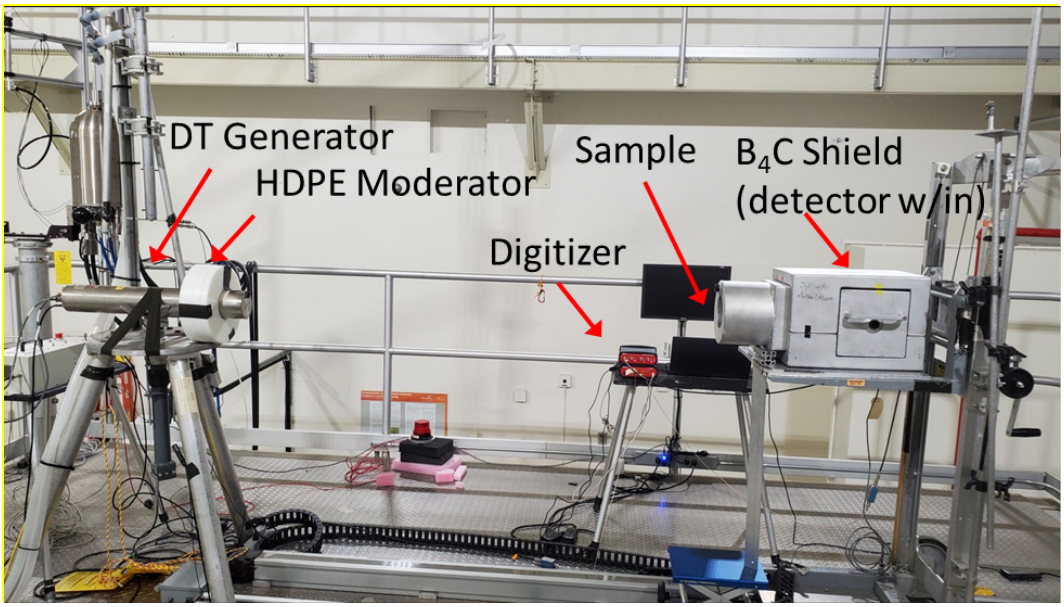

Figure S 1. Photograph of the pNRTA experimental setup at PNNL. All components are commercial off-the-shelf except the custom moderator and B_4C shield.

The modeling, experiments, and analysis executed in this project demonstrate that pNRTA is feasible for assaying ^{232}Th, ^{233}U, ^{235}U, and other isotopes in many forms, including metals, ceramics, salts, and even liquids. Table S 1 contains a summary of material forms and isotopes examined in the project. The pNRTA prototype shows significant promise as a new capability for non-destructive assay (NDA) for thorium fuel cycle safeguards.

Table S 1. Sample forms and compositions either measured or simulated in the project.

Target	Meas. Time (min)	Isotopes	Accessible with pNRTA?
^{233}U oxide (1.2 mm)	150	^{233}U	Yes, low (2.5%) measured bias
^{232}Th metal (3 mm)	60	^{232}Th	Yes
^{232}Th + DU metal	120	^{232}Th/^{235}U/^{238}U	Yes
^{232}Th + HEU metal	120	^{232}Th/^{234}U-^{238}U	Yes
^{233}U + HALEU (0.6 mm)		^{233}U-^{238}U	Yes
^{233}U + HALEU + ^{232}Th	180	^{232}Th/^{233}U-^{238}U	Yes
Simulated Shippingport Reactor Fuel Pellets (Taylor and Loo 1999)	60	^{233}U, ^{232}Th	Yes
Simulated Molten Salt Reactor Fuel, 0.137 mol % $^{233}UF_4$, 3- 10 mm (Houtzeel and Dyer 1972)	60	^{233}U, ^{232}Th	No, low U concentration
Simulated Molten Salt Fast Reactor Fuel, 2.5 mol % $^{233}UF_4$, 10 mm (Heuer et al. 2014)	60	^{233}U, ^{232}Th	Yes
High U concentration acid (400 g ^{233}U/L) (10 mm)	60	^{233}U	Yes

Key findings include:

Modeling & Simulation: A high-fidelity MCNP model was developed, refined, and benchmarked with experimental data. It was used to simulate TOF spectra for a range of targets relevant to thorium fuel cycle safeguards and conduct sample parameter studies. Assessed pNRTA's ability to measure a range of different MSR compositions and sizes.

Detector Study: A detector evaluation study identified promising alternative detectors to GS20 for irradiated and non-irradiated samples. Initial measurements with CLYC showed improved uncertainty in TOF spectra compared with GS20 for samples with higher radioactivity thanks to CLYC's far superior neutron/gamma discrimination capability. Irradiated samples will require a neutron detector with very low gamma-ray sensitivity and accurate neutron/gamma-ray discrimination. The most promising detectors identified for this purpose were ^{3}He and stacked BCS. A multi-element stacked BCS detector was designed and determined via simulations to have similar efficiency as 5 mm of GS20. BCS and ^{3}He detectors were assessed in high gamma fields expected from irradiated samples.

Measurements & Analysis: The team measured and analyzed unique data set of gram-level U/Th targets in different configurations, including the first ever pNRTA measurements of ^{233}U and HALEU. Measurement times ranged from 60-180 min. REFIT was used to analyze experimental and simulated TOF spectra. Assay precision decreased proportionally with sample radioactivity with the GS20 detector due to increased gamma-ray backgrounds. This was most evident with the ^{233}U samples, which required up to 25 mm of lead shielding and decreased the neutron signal. Repeat measurement uncertainty over several months for one sample was ~10%. A custom, open-source analysis algorithm (NeuFIT) was developed, which showed similar performance as REFIT with understanding of how the program works. For the set of 15

isotope assays (from measurements of eight targets), the mean bias and RSD were 9% and 36%, respectively. Individual assay results with NeuFIT are shown in Table S 2.

Table S 2. NeuFIT assay results for measured target configurations. Z = (predicted-true)/(predicted error), is a measure of the prediction error relative to the predicted value.

Target	Time (min)	Isotope	Predicted Abund. (at/b)	True Abund. (at/b)	% Diff	Z
Th	120	232Th	$1.12 \pm 0.03 \times 10^{-2}$	0.91×10^{-2}	23.1%	7.0
UO_2, sample 1	150	233U	$2.55 \pm 0.37 \times 10^{-4}$	$3.22 \pm 0.36 \times 10^{-4}$	-20.8%	-1.8
UO_2, sample 2	180	233U	$2.89 \pm 0.42 \times 10^{-4}$	$3.10 \pm 0.34 \times 10^{-4}$	-6.8%	-0.5
Both UO_2, samples	180	233U	$4.81 \pm 0.54 \times 10^{-4}$	$6.32 \pm 0.50 \times 10^{-4}$	-23.9%	-2.8
Th + UO_2 samples	180	232Th 233U	$1.97 \pm 0.71 \times 10^{-2}$ $4.47 \pm 0.54 \times 10^{-4}$	0.91×10^{-2} $6.32 \pm 0.5 \times 10^{-4}$	116.5% -29.3%	1.5 -3.4
HALEU	180	235U 238U	$1.39 \pm 0.28 \times 10^{-3}$ $5.59 \pm 1.11 \times 10^{-3}$	1.44×10^{-3} 5.73×10^{-3}	-3.5% -2.4%	-0.2 -0.1
UO_2 samples + HALEU	180	233U 235U 238U	$5.02 \pm 0.59 \times 10^{-4}$ $1.40 \pm 0.39 \times 10^{-3}$ $7.09 \pm 1.98 \times 10^{-3}$	$6.32 \pm 0.5 \times 10^{-4}$ 1.44×10^{-3} 5.73×10^{-3}	-20.6% -2.8% 23.7%	-2.2 -0.1 0.7
Th + UO_2 samples + HALEU	180	232Th 233U 235U 238U	$1.29 \pm 1.13 \times 10^{-2}$ $6.05 \pm 0.74 \times 10^{-4}$ $1.69 \pm 0.55 \times 10^{-3}$ $7.50 \pm 2.42 \times 10^{-3}$	0.91×10^{-2} $6.32 \pm 0.50 \times 10^{-4}$ 1.44×10^{-3} 5.73×10^{-3}	41.8% -4.3% 17.4% 30.9%	0.3 -0.4 -0.4 0.7

Acknowledgments

This research was supported by the National Nuclear Security Agency's Office of Defense Nuclear Nonproliferation Research & Development. This project benefited by standing on the shoulders of the Isotope Verification for Arms Control (IVAC) project, which developed the initial pNRTA prototype and optimized the neutron moderator. Ethan Klein was also supported in part by an appointment to the Nuclear Nonproliferation International Safeguards Fellowship Program sponsored by the National Nuclear Security Administration's Office of International Nuclear Safeguards (NA-241). MIT was funded in part by the NNSA's Consortium on Monitoring and Verification (CVT) University Program.

Many additional staff helped make this project successful and are gratefully acknowledged for their programmatic, logistical, or technical support: Andy Gilbert, Jonathan Burnett, Bruce Pierson, Kevin Bertschinger, Richard Clark, Sergey Sinkov, Andrew Maine, Mary Bliss, and Warnick Kernan.

Acronyms and Abbreviations

BCS	Boron coated straw
DD	Deuterium deuterium
DT	Deuterium tritium
DU	Depleted uranium
ENDF	Evaluated nuclear data file
HALEU	High assay low enriched uranium
HDPE	High density polyethylene
HPGe	High purity germanium
HEF	High Exposure Facility
HEU	Highly enriched uranium
iNEUIT	iNEUtron Imaging Toolbox
IVAC	Isotope Verification for Arms Control
MDC	Minimum detectable concentration
MIT	Massachusetts Institute of Technology
MSR	Molten salt reactor
MSRE	Molten Salt Reactor Experiment
NDA	Non-destructive assay
LEU	Low enriched uranium
LSF	Low Scatter Facility
MCNP	Monte Carlo N-Particle
NRCA	Neutron resonance capture analysis
PNNL	Pacific Northwest National Laboratory
pNRTA	portable Neutron resonance transmission analysis
RMT	Radioactive Materials Tracking
TOF	Time of flight
TRL	Technology readiness level

Contents

Figures

Tables

This page intentionally left blank.

1.0 Introduction

Emerging thorium fuel cycles present new challenges for safeguards measurements, chiefly by the introduction of ^{233}U and its co-abundance with other safeguards-relevant isotopes. This project set out to develop and demonstrate portable neutron resonance analysis (pNRTA) as a new method for quantitative assay of ^{233}U, ^{235}U, ^{232}Th, and other isotopes when they are present together in a sample. The project set out to achieve several key research objectives:

1. Demonstrate the feasibility of pNRTA for ^{233}U and ^{235}U assay by performing modeling and laboratory experiments with relevant samples. This includes incorporating a neutron detector that can discriminate neutrons from gamma-rays in high gamma fields and developing quantitative algorithms to analyze pNRTA data.

2. Raise the technology readiness level (TRL) of pNRTA by performing measurements on representative samples in a laboratory setting and show how it could be practical for safeguards.

3. Show how gamma-ray signatures can complement pNRTA for enhanced assay performance, such as by constraining materials in a sample. This includes passive gamma-ray singles and coincidence spectroscopy and Neutron Capture Resonance Analysis (NRCA).

The research team decisively achieved the first two objectives, providing a technical basis for future development of pNRTA and potential use in thorium fuel cycle safeguards. The third objective was explored to a lesser degree after guidance from mid-project Independent Assessment committee encouraged the team to focus on pNRTA. The team at MIT made strides developing NRCA for this application and how it may complement pNRTA.

This report summarizes the key outcomes and final results since completion of the mid-project report (B. McDonald, Burnett, Clark, Danagoulian, Gilbert, Klein, et al. 2022). Section 2.0 includes a short background of related efforts, and a summary of material forms and compositions that can be assayed with pNRTA. Section 3.0 describes new modeling results for different material forms and concentrations, Section 4.0 describes detector requirements and considerations for thorium fuel cycle NRTA and gamma-ray measurements. Section 4.5 summarizes preliminary measurements and analysis, including characterizing of ^{233}U material at PNNL. Section 5.4 describes progress with quantitative isotopic analysis algorithms. The last section summarizes key findings for the project and ways to increase the technology readiness level (TRL) of pNRTA.

2.0 Background

2.1 Project Context and Method Applicability

This project built upon a pNRTA capability developed at PNNL in the “Isotope Verification for Arms Control” project (IVAC, FY21-PL-PD2Nc-P18) and pioneering pNRTA work at MIT (E. Klein et al. 2021; Engel, Klein, and Danagoulian 2020; Zalavadia et al. 2021). An overview of basic NRTA theory, analysis, and details related to safeguards measurements is found in (Benjamin S McDonald et al. 2024). A photo of some of the project team is in Figure 1.

Figure 1. From left to right: Mital Zalavadia, Jon Kulisek, and Michael Moore (PNNL), and Ethan Klein, Areg Danagoulian, and Farheen Naqvi (MIT). Dr. Naqvi was not part of this effort, and all three were visiting as part of the prior project.

NRTA (sans ‘portable’) was developed fifty years ago to assay spent nuclear fuel (Priesmeyer and Harz 1975). It is chiefly non-destructive, isotope-specific, quantitative, and can perform in high radiation environments. It can be performed in imaging or non-imaging modes and can determine the areal density or mass of isotopes with detectable resonances in the applicable energy range of the system (e.g., 1-100 eV). Until recently, it has been confined to large accelerator-based facilities with <8 m neutron flight paths — a decidedly non-portable method. NRTA has been considered for safeguards applications in that fixed-facility context. (Paradela et al. 2017; Chichester and Sterbentz 2012) A modern example of exquisite, 3D isotopic mapping of a nuclear fuel pellet is found in (Losko and Vogel 2022). These and other time-of-flight (TOF) spectra from large-scale NRTA experiments have sharp resonances (“high resolution”), whereas pNRTA TOF spectra have coarser resolution. As an analogy with gamma-ray spectrometry, it is as if only lab-based high-purity germanium detectors existed, and medium-resolution and portable detectors were just created. pNRTA similarly offers a new way of doing verification in typical labs and in field measurements untethered from large, fixed facilities.

Several recent efforts have considered and evaluated existing, currently used safeguards NDA techniques for thorium fuel cycle safeguards. A 2021 report noted that quantitative assay of ^{232}Th with neutrons was difficult or impractical (Evans et al. 2021). Further, assay of ^{233}U was considered possible with some existing techniques, but it was not clear if these would be able to

assay ^{233}U and ^{235}U together. That has been the focus of a multi-lab project that ran in parallel with this one. That project demonstrated several ways to assay ^{233}U oxide samples (Searfus et al. 2023). These showed promise for pure samples and for certain material forms. For samples containing ^{233}U and ^{235}U, an active well coincidence counting system could only determine the total fissile mass and not the quantities of the individual fissile isotopes. (Lockhart et al. 2025). Tests were done with ^{233}U and ^{235}U samples with masses of each up to around 80 g.

Table 3 shows the predicted assay feasibility with current techniques from the Evans report next to pNRTA results from this project. Note that a column original to the Evans report on passive assay was removed (all were 'not feasible'). Because the uranium and thorium isotopes of interest have at least some distinct neutron resonances, pNRTA is applicable for likely all the material types and assay targets considered. Moreover, pNRTA is also sensitive to additional isotopes that are of safeguards interest (e.g., ^{233}Pa and ^{239}Pu). Additional material forms (e.g., liquids) and an assay target (i.e., composite $^{233}U/^{235}U$) were also added to the table.

Table 3. Summary of the evaluation of the feasibility of neutron NDA techniques with pNRTA included, adapted from (Evans et al. 2021).

Assay Target	Material type	Active Assay	Self-Interrog.	pNRTA
^{232}Th	^{232}Th metal	Difficult, fast neutrons only	Not feasible	Experimentally demonstrated
	$^{232}ThO_2$	Difficult, fast neutrons only	Not feasible	Demonstrated in silico
	(^{233}U, Th)O_2	Not feasible	Not feasible	Demonstrated in silico
	(Enriched U, Th)O_2*	Not feasible	Not feasible	Demonstrated in silico
	ThC*	Difficult, fast neutrons only	Not feasible	Not examined
	Th(FLiBe) salt*	Difficult, fast neutrons only	Not feasible	Demonstrated in silico
^{233}U	^{233}U metal	Feasible, similar to ^{235}U	Not feasible	Demonstrated in silico
	$^{233}UO_2$	Feasible, similar to ^{235}U	Difficult, potentially feasible	Experimentally demonstrated
	$^{233}UF_4$	Feasible, similar to ^{235}U	Likely feasible	Not examined
	^{233}U in acid			Demonstrated in silico
^{235}U	^{235}U metal			Experimentally demonstrated
	$^{235}UO_2$			Demonstrated in silico
	$^{235}UF_4$			Not examined
^{233}U/^{235}U	U metal			Demonstrated in silico
	$^{233}UO_2$ + ^{235}U metal			Experimentally demonstrated
	UF_4			Not examined

*Material type not included in the simulations or measurements of Evans et al report.

As shown in more detail in the ensuring chapters, pNRTA is applicable to many materials and forms including salts, metals, ceramics, and even liquids in suitable form factors. Sample dimensions should ideally cover the field of view of the collimated detector. Samples should have sufficient areal density to attenuate probing neutrons (i.e., one or more path lengths), typically on the order centimeters for most samples. Hydrogenous samples, which may have high neutron scattering and absorption cross-sections, can degrade TOF resolution. That said, simulations with thin liquid, high-uranium concentration acids, and salt compositions expected in advanced reactor fuel cycles, shows that they could be assayed with pNRTA.

2.2 System Overview

The pNRTA system consists of nearly all commercially available components, except for a custom moderator assembly and detector shielding components. It fits within several man-portable cases. A photograph of the setup at the PNNL 318 Building, Low Scatter Facility (LSF)

is shown in Figure 3. A Thermo Scientific™ P 385 deuterium-tritium (DT) neutron generator (at left in Figure 3) creates 14.1 MeV neutrons that are moderated in a custom lead and high-density polyethylene (HDPE) collars (Figure 4). Photos of the DT generator and moderator are shown in Figure 4. The moderator enhances epithermal neutron production while reducing the spread in moderation time, which impacts overall system resolution [more detail in (Zalavadia et al. 2021)]. The IVAC project determined settings for the pulse structure of the generator to limit 'wrap-around' neutrons and maintain high flux rates. The generator pulse frequency was 5000 Hz with a duty factor of 3.5%. Of the nominal 7 μS pulse width, the actual pulse widths were closer to 1 μS . Typically, the DT generator was run at 130 kV and 35 μA for measurements less than 2 hours. Moderated neutrons drift across a 2.0 m distance and pass through a sample placed in front of a collimated detector shield assembly (at right in photo). Between the sample and the detector, a 3 mm thick cadmium cap enclosed in aluminum was acquired to limit thermal neutrons impinging on the detector. Neutrons are attenuated depending on the sample isotope's macroscopic cross-section and then detected by a detector. A 5 mm thick GS20 (Scintacor, Inc) ^{6}Li glass scintillator coupled to a ø7.6 cm photomultiplier tube (PMT) was the standard detector in most experiments. The detector was placed inside a B_4C shield that reduces off-axis neutrons (e.g., room return) and readout by a CAEN digitizer (DT5730SB). The timing signal from the DT generator pulse was fed into the digitizer, which computed the difference between the neutron pulse and the detector signals as the time of flight for each event in 250 ns bins. A CAEN supply provided high voltage bias to the PMT.

Figure 2. Cutaway view of the 318 Building REM Lab. The pNRTA experiments were setup on the raised platform near the center of the rendering.

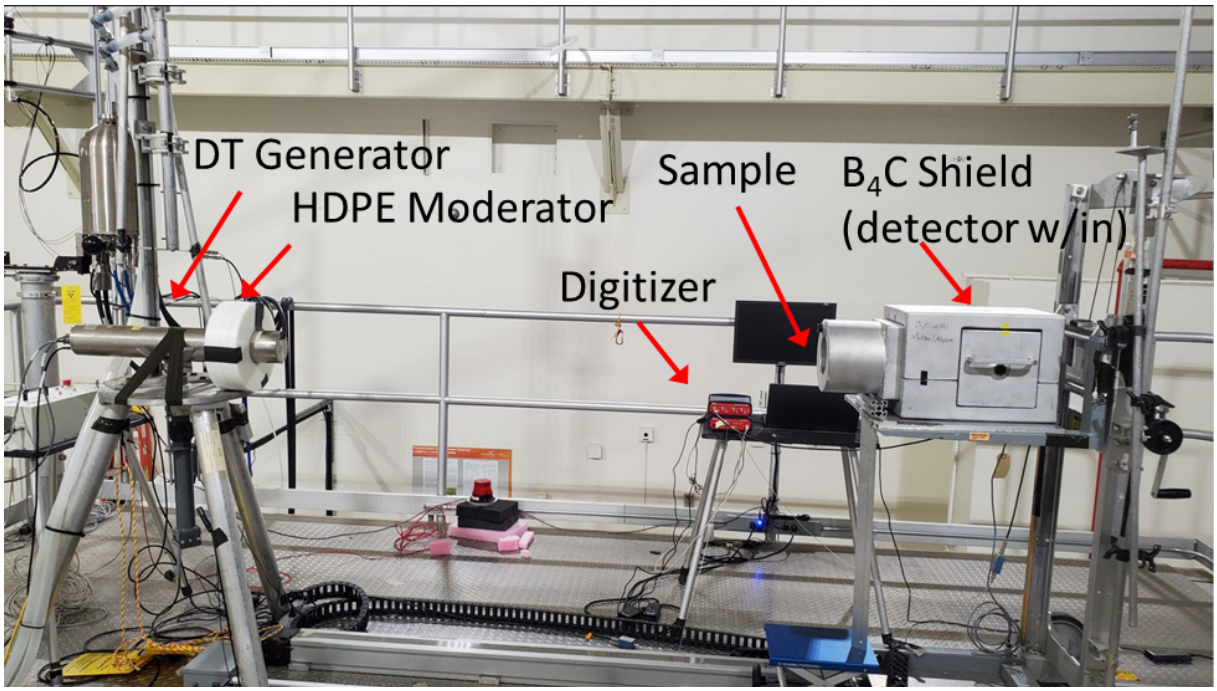

Figure 3. Photograph of the PNNL pNRTA setup with 2.00 m standoff.

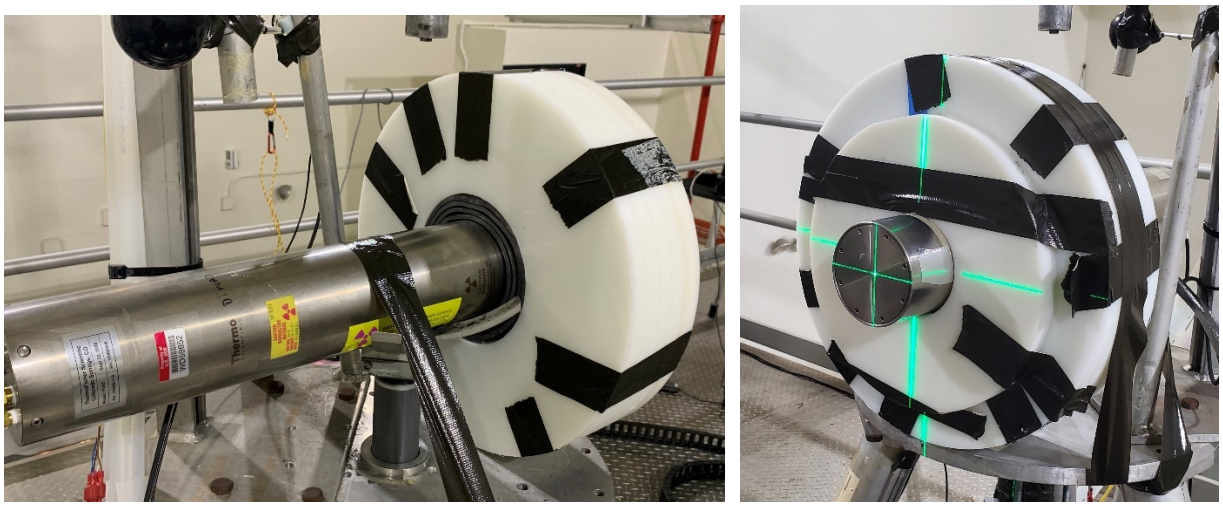

Figure 4. Photos of the DT generator with custom lead/HDPE annuli from rear (left) and front (right) views.

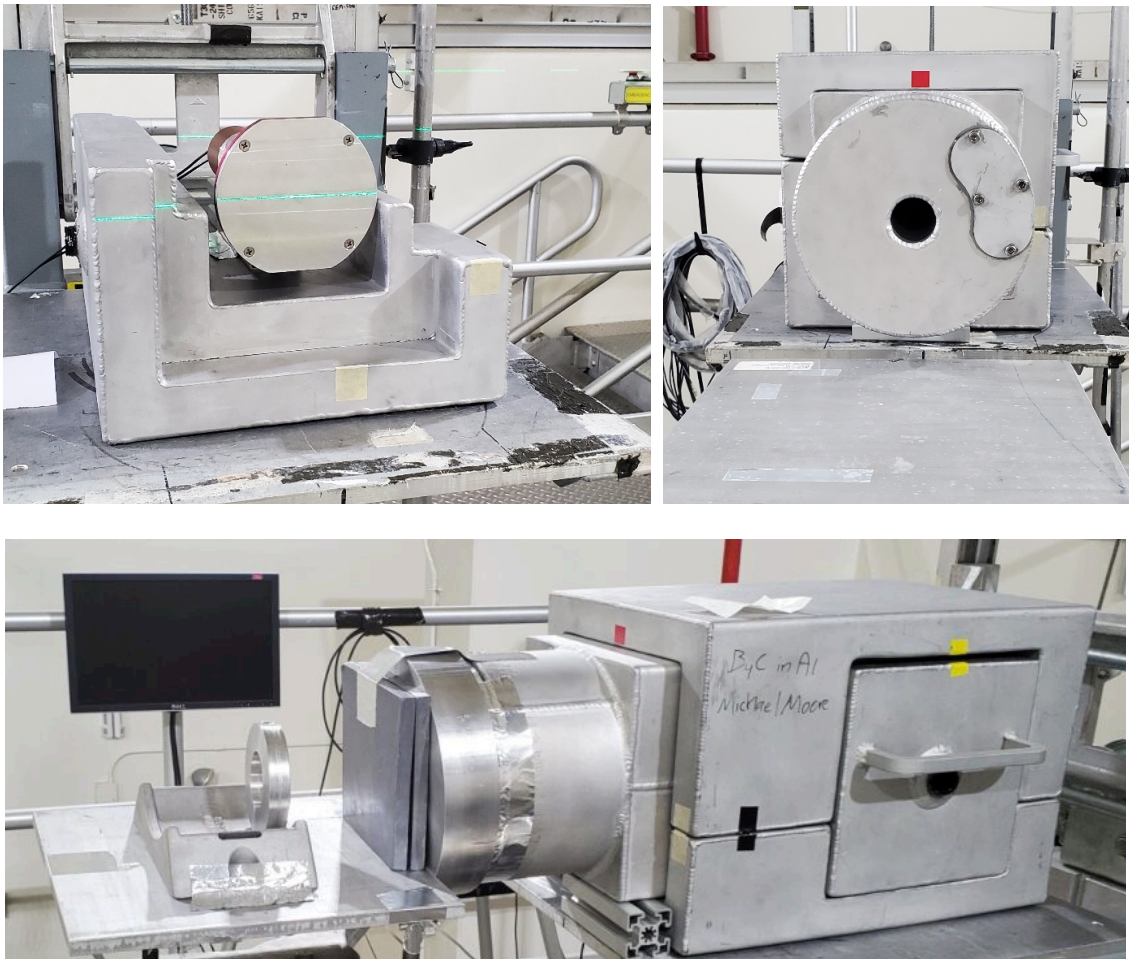

Figure 5. Photos of the GS20 detector within the B_4C shield (top left), the assembled shield with ø42 mm collimator insert attached (top right), and full setup with a 233U target, lead shielding, and cadmium cap (bottom).

A very similar pNRTA system at MIT, shown in Figure 6, was used throughout the project for complementary investigations. Most results in this report are from data collected with the PNNL system. A cartoon applicable to both setups is shown in Figure 7.

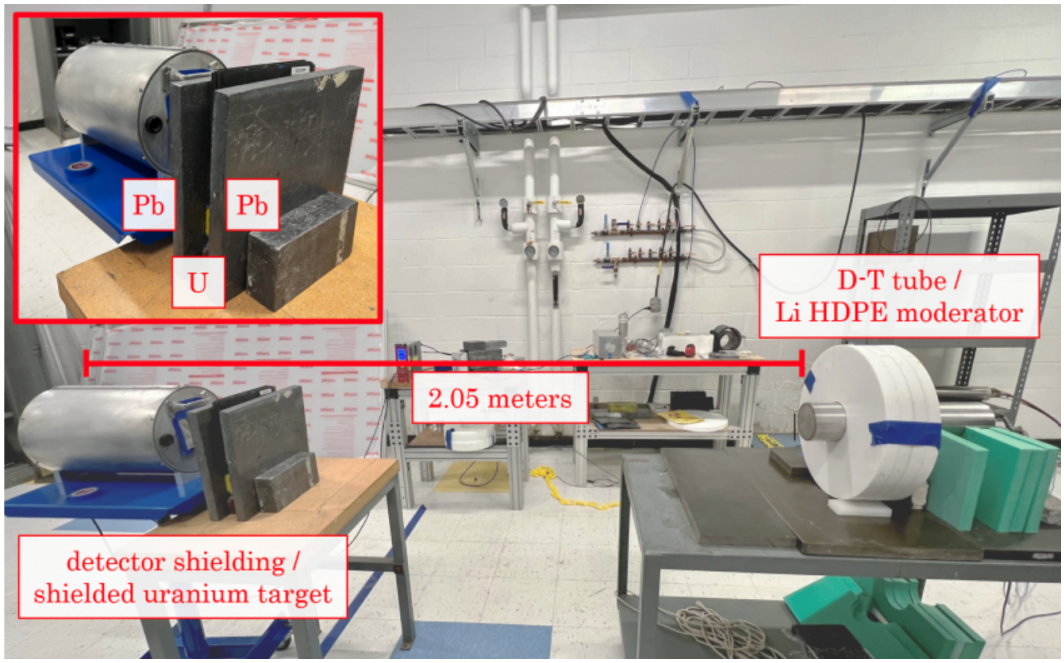

Figure 6. Photo of the pNRTA experimental setup at MIT with a depleted uranium target. (Shayaan Subzwari, Rahon, et al. 2024).

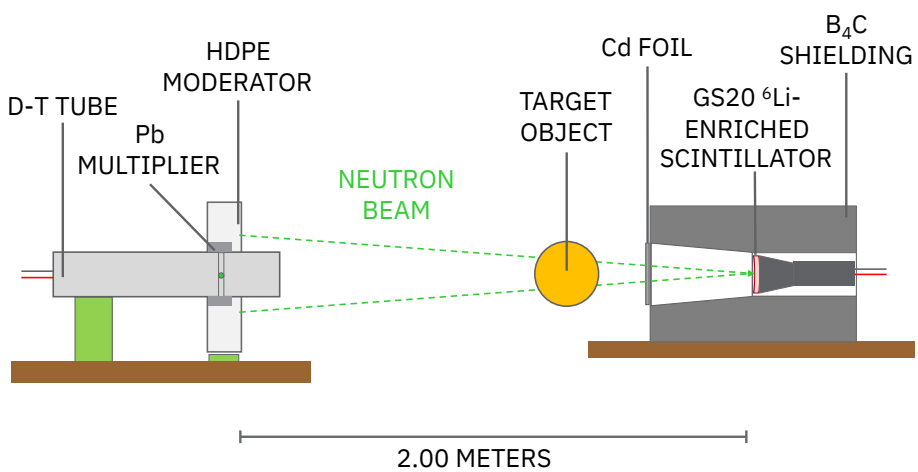

Figure 7. Cartoon of the pNRTA setups at both PNNL and MIT.

3.0 Modeling and Simulation

MCNP6.2® (MCNP) was used to conduct all the radiation transport simulations (Werner et al. 2018). A detailed description of the model was provided in the mid-project report (B. McDonald, Burnett, Clark, and Danagoulian 2022). This section provides several important updates, including model benchmarking with measured data, a parameter study that varied the fractions of U-233 and U-235, a study investigating the detectability of U-233 in molten salts, potential interferences from fission products in molten salts, and a brief exploration of pNRTA's applicability to assaying liquids and ceramics containing nuclear material.

3.1 Model Benchmarking

The MCNP model was benchmarked with experimental data from this project (Figure 8) and several nuclear material targets in the IVAC project not shown here (e.g., DU, HEU, Pu. Agreement across the TOF spectra was shown to be better than 20% for each timing bin. The passive gamma-ray background was subtracted from these spectra. An offset to align the measured and modeled spectra and the source strength were calculated by fit: MCNP×*Source* + *Offset* = Measurement. In the open beam and thorium target runs, the offsets were 206.1 and 205.6 counts/bin, respectively. The source intensities were within range for the expected neutron generator output settings. These results provided confidence that the model was producing results congruent with measurements with the GS20 detector. Note that in both figures a time offset of 7.5 μs was added to match with the experimental offset. Without the offset the ^{232}Th resonances would be near 31 μs.

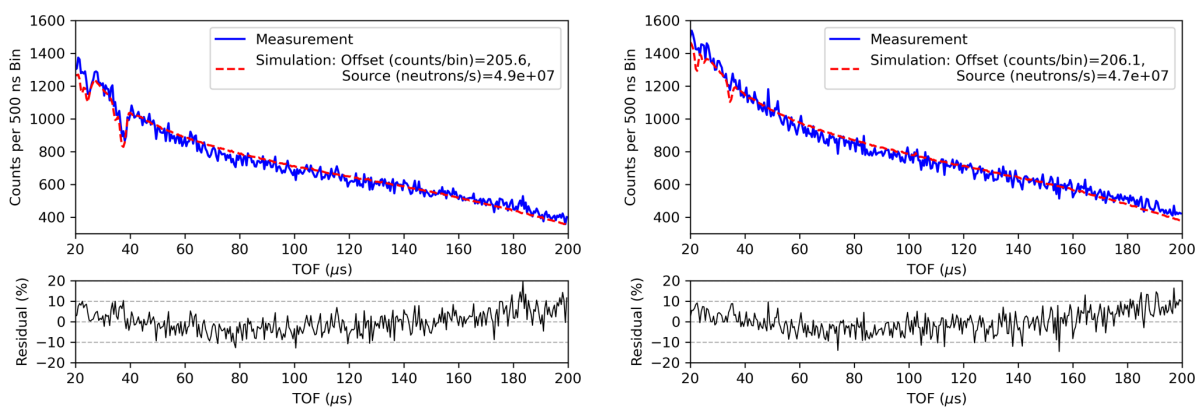

Figure 8. Measured and simulated data for the ^{232}Th target (left) and open beam (right).

3.2 ^{233}U/^{235}U Parameter Studies

Expanding from simulations described in the mid-project report, TOF spectra of varying ^{233}U/^{235}U concentrations (0.1 to 99.9 wt.% ^{233}U, with the balance being ^{235}U) and thicknesses 1-10 mm) for metal targets were generated to assess the sensitivity of the current system for these isotopes for different sample thicknesses. Figure 2 shows example TOF spectra for a 4 mm thick metal sample. At the largest times (lowest energies) the ^{233}U resonances are the strongest (most attenuating) and this is also where the system resolution is the highest. As the ^{233}U level increased from 20 to 99.9 wt.%, the two resonances at ~120 and 140 μs disappeared into the continuum. This happens when attenuation by the sample dominates and only

background terms remain. Thus, the maximum areal density of ^{233}U that can be interrogated with this system at those energies is somewhere in the range of 1.5-7.6 g/cm^2.

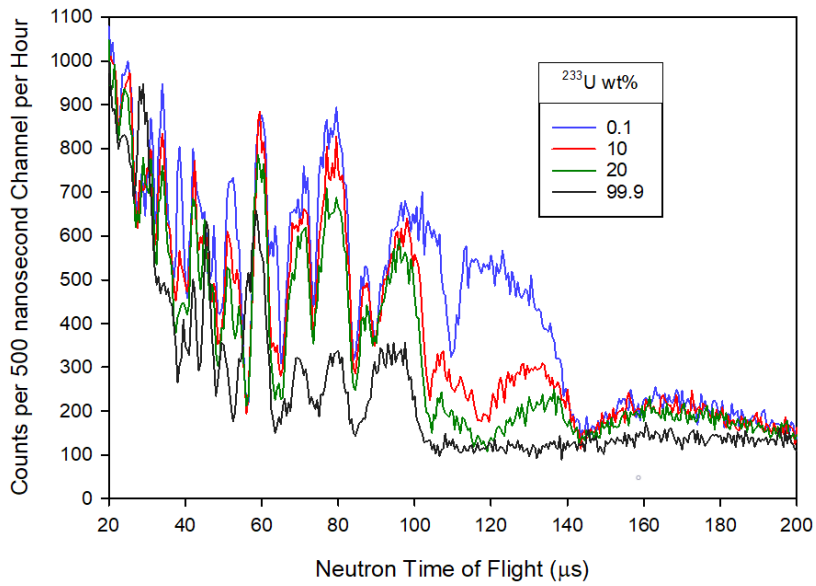

Figure 9. Simulated TOF spectra a metal targets with 4 mm thickness and varying $^{233}U/^{235}U$ concentrations. Poisson noise was added to these simulated results.

3.3 Molten Salt Reactor Fuel

Compositions of several molten salt reactor (MSR) fuel materials were identified in the literature and used in MCNP simulations to assess whether pNRTA can assay their safeguards-relevant isotopes. As a first look, the Oak Ridge National Laboratory (ORNL's) iNEUtron Imaging Toolbox) program (Zhang et al. 2019; Zhang and Bilheux 2017) was used to rapidly generate TOF spectra for four different molten salt fast reactor fuel compositions (Heuer et al. 2014). These spectra were convolved with the timing resolution of the pNRTA prototype system and are shown in Figure 10.

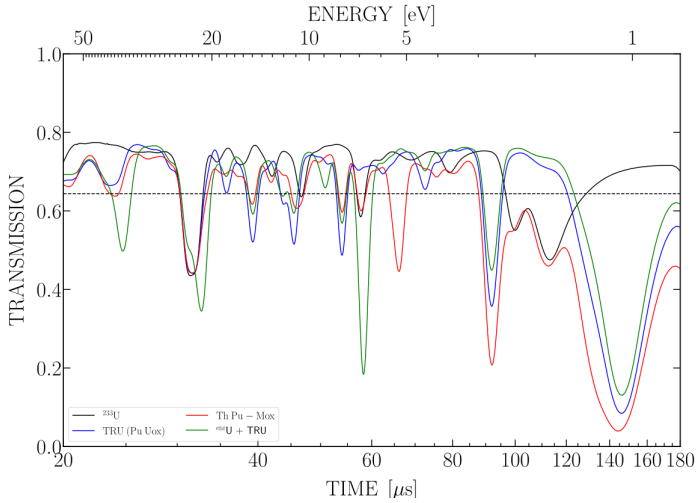

Isotope	^{233}U	TRU (Pu Uox)	Th Pu-Mox	^{enr}U + TRU
^{7}Li	6.1	6.1	6.1	6.1
^{19}F	35.6	35.6	35.6	35.6
^{232}Th	51.8	41.55	37.30	20.74
^{231}Pa	-	-	0.041	-
^{232}U	-	-	0.002	-
^{233}U	6.61	-	4.70	-
^{234}U	-	-	0.65	-
^{235}U	-	-	0.092	3.55
^{236}U	-	-	0.027	-
^{238}U	-	-	-	24.06
^{237}Np	-	1.08	0.11	0.68
^{238}Pu	-	0.47	0.64	0.30
^{239}Pu	-	7.95	2.83	5.04
^{240}Pu	-	3.74	5.39	2.37
^{241}Pu	-	1.87	0.605	1.18
^{242}Pu	-	1.17	2.83	0.75
^{241}Am	-	0.59	2.90	0.38
^{243}Am	-	0.33	0.72	0.21
^{244}Cm	-	0.14	0.11	0.09
^{245}Cm	-	0.01	-	0.008

Figure 10. TOF transmission spectra of four MSR fuel compositions (left) and their respective isotopic compositions (right). Table is from (Heuer et al. 2014) in mol. %.

First, the team modeled a sampled of molten salt with fission product concentrations as measured in the Molten Salt Reactor Experiment (MSRE) (Compere et al. 1975). No resonances were seen from uranium or fission products in samples ~ 3 mm and 10 mm thick (Figure 11). While it is helpful that the salts and fission products do not create any interfering resonances, the lack of resonances from uranium isotopes is concerning. In another effort, researchers found that six fission products in spent solid fuel assemblies created strong resonances in NRTA TOF spectra: ^{99}Tc, ^{103}Rh, ^{131}Xe, ^{133}Cs, ^{145}Nd, and ^{152}Sm (Chichester and Sterbentz 2012). The fission product concentration in the MSRE was likely much lower than the spent fuel compositions in the 2012 report because of lower burnup and the way fission products persist in the different fuel matrices. The uranium concentration in the MSRE was low (0.137 mole % $^{233}UF_4$) compared with some of new designs with molten salts (2.5 mole % $^{233}UF_4$) (Heuer et al. 2014). shows that NDA of uranium in some salts may not be feasible with pNRTA. Larger sample thicknesses are possible due to the low attenuation properties of the salts. We simulated 10-cm thick samples for the MSRE and 2.5 mol% Heuer et al examples and determined that the former still did not provide discernable resonances, but the latter did. Even thicker samples may be warranted to increase detectability of ^{233}U and/or ^{235}U in MSR samples. Note the resonance at 27.4 eV is from the ^{111}Cd thermal neutron filter and present in most TOF spectra because of the 3 mm Cd cap on the detector collimator opening.

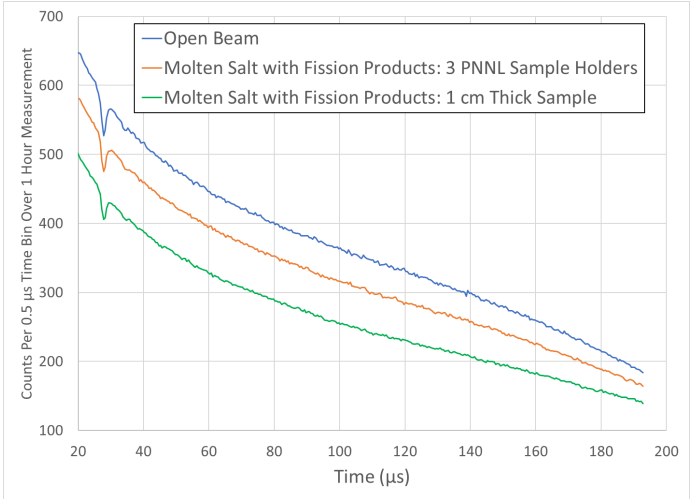

Figure 11. Simulation results of MSRE samples with ~3 mm (red) and 10 mm (green) thickness and open beam (blue).

Table 4. Fission product concentrations modeled taken from the MSRE.

Isotope	Bq per gram of salt	Wt.% of salt
Sr-89	7.98E+08	7.43E-05
Y-91	1.41E+09	1.56E-04
Ba-140	1.47E+09	5.42E-05
Cs-137	8.10E+07	2.52E-03
Ce-141	1.34E+09	1.27E-04
Ce-144	1.01E+09	8.53E-04
Zr-95	1.27E+09	1.60E-04
Nb-95	7.27E+07	4.99E-06
Mo-99	1.90E+09	1.07E-05
Ru-103	5.83E+07	4.88E-06
Ru-106	4.83E+06	3.94E-06
Ag-111	1.93E+06	3.31E-08
Te-129m	2.48E+07	2.23E-06
Te-132	4.40E+08	3.85E-06
I-131	3.95E+08	8.59E-06

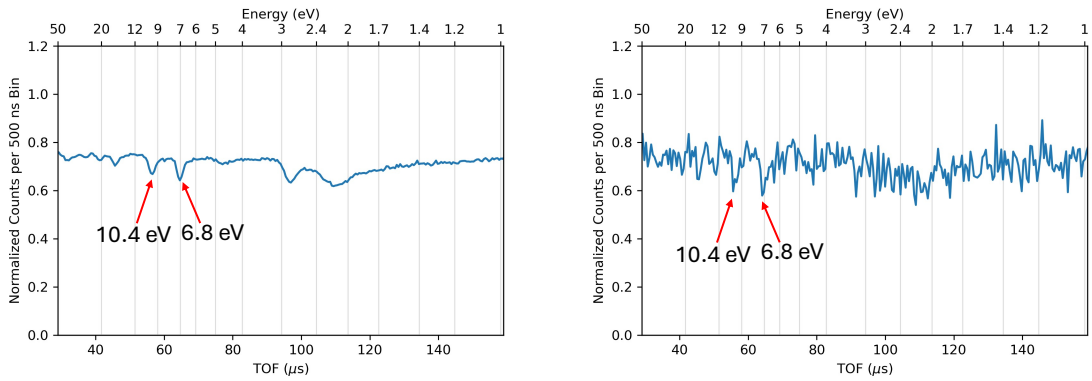

Figure 12. Simulated TOF transmission spectra through a 10 cm sample of 2.5 mol% $^{233}UF_4$ molten salt. (Left) No noise from counting statistics, (Right): Noise expected from a 1-hr measurement.

We next considered an initial fuel salt composition for an MSR fuel with 19.79 wt.% ^{235}U (remainder as ^{238}U), where the highest to lowest molar percentages were LiF (70.19%), BeF_2 (15.65%), ThF_4 (70.19%), and UF_4 (2.44%) (Betzler, Wieselquist, and Fratoni 2020). A 1-cm thick sample with density 1.9 g/cm^3 was modeled. In Figure 13, Figure 13the detected resonances from ^{232}Th and ^{238}U are discernible. The largest dips in the TOF spectrum at 6.7 eV (~65 μs) and ~22 eV (~40 μs) are from ^{238}U and overlapping ^{232}Th and ^{238}U resonances, respectively. Importantly, the low atomic number constituents of the salt do not significantly attenuate the epithermal neutrons. A thicker sample would likely be needed to observe ^{235}U resonances.

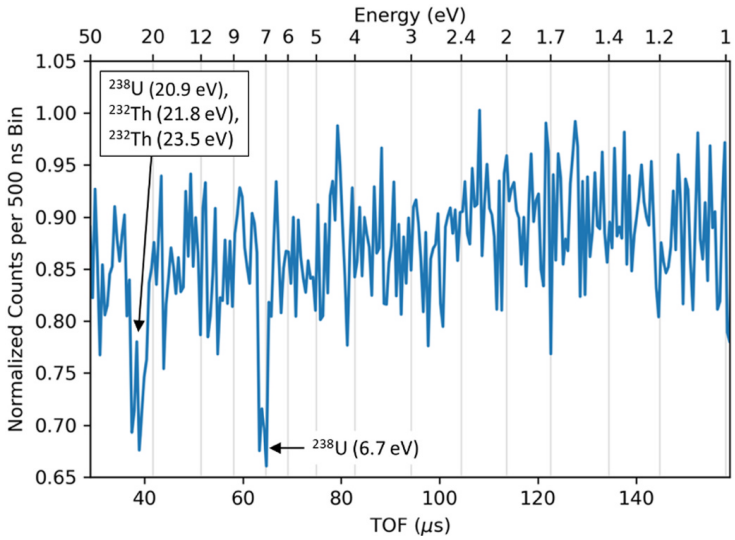

Figure 13. Neutron transmission versus TOF and energy in a GS20 neutron detector for a 1 cm thick nominal MSR initial fuel salt. Poisson noise is included in this spectrum based on the total simulated counts within each channel over a one-hour long neutron irradiation.

3.4 UO_2-ThO_2 Fuel

The team made pNRTA simulations of two uranium-thorium composite fuels from the literature. First, Shippingport breeder reactor seed fuel rod elements were modeled (Taylor and Loo 1999). The purpose of these simulations was to determine the feasibility of measuring a sample mixture of ^{233}U and ^{232}Th together in breeder reactor fuel. The Shippingport reactor seed fuel was a mixed oxide of UO_2-ThO_2, which consisted of 5.2 wt.% ^{233}U and 82.6 wt.% ^{232}Th (both weight percentages being with respect to the total fuel mass). The diameter was 6.4 mm with density of ~10 g/cm^3. Overall, these were a higher areal density of uranium than simulated so far. These represented an interesting test case. Four of these fuel rods were modeled side-by-side over the aperture of the B_4C shield containing the GS20 detector, as shown by the four small blue circles at the far left in the inset in Figure 14. An hour-long assay of these rods was simulated. The simulated TOF spectrum, shown in Figure 14, contains easily discernable ^{232}Th and ^{233}U resonances. Resonances for ^{233}U and ^{232}Th are visible at 100-120 μs and 40 μs, respectively, showing that assay these sample types are accessible with pNRTA. Overall, this exploration indicated that the pNRTA prototype system can assay these isotopes in relevant nuclear pellet/rodlet configurations in hour-long assay times.

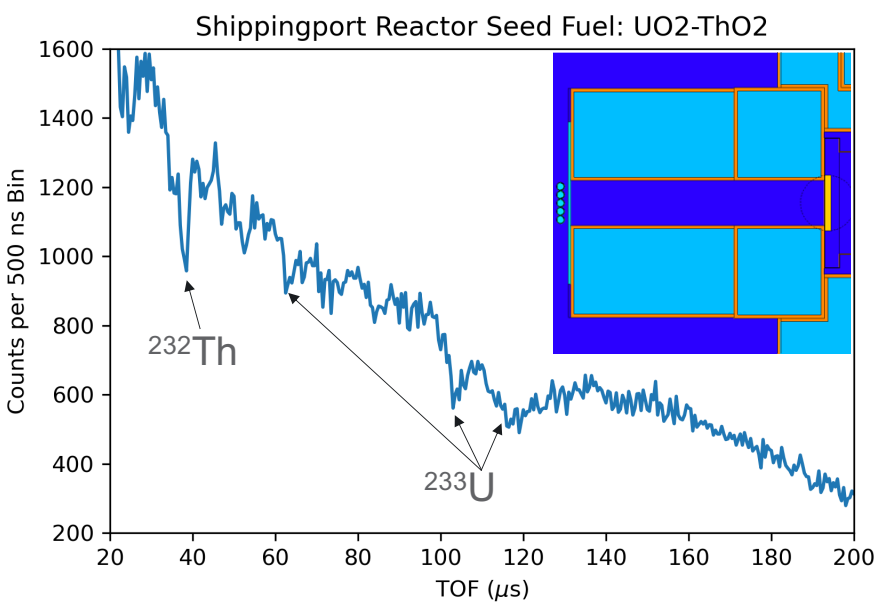

Figure 14. Results of the simulated 1-hour long NRTA assay of four Shippingport breeder reactor fuel rod elements. The figure inset, a top view 2D cross section, illustrates how the fuel rod elements (four small circles at the far left) were modeled with respect to the B_4C shield.

The team next modeled another case of UO_2-ThO_2 fuel that is distributed with MCNP in the Whisper package (U233-COMP-THERM-004). These were 2.6 wt.% ^{233}U and 85.2 wt.% ^{232}Th fuel rod sections, similar to the Shippingport material, but with roughly half the ^{233}U content. The simulated TOF spectrum is shown in Figure 15. The lack of defined ^{233}U resonances indicate that 2.6 wt.% may be near the sensitivity limit of the system and/or longer measurement times are needed.

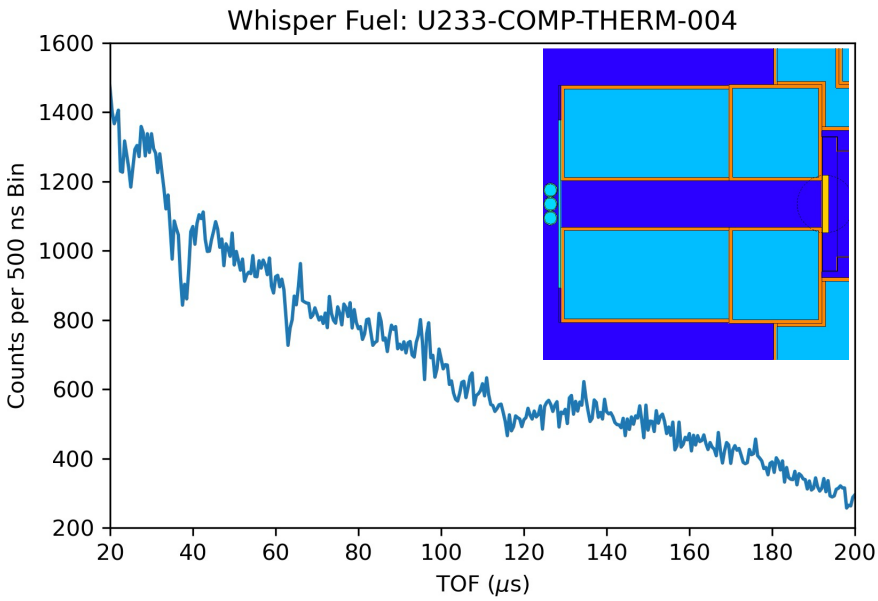

Figure 15. Results of the simulated 1-hour long NRTA assay of three elements from Whisper. The figure inset, a top view 2D cross section, illustrates how the fuel rod elements (three small circles at the far left) were modeled with respect to the B_4C shield.

3.5 Liquids with High Concentrations of Uranium

An MCNP simulation was conducted of the assay of a 1-cm thick liquid sample consisting of 400 g of ^{233}U per liter, a NHO_3 molarity of 2.0 mol per liter, and density of 1.6 g/cm^3. The purpose of this analysis was to determine the applicability of the NRTA method to liquid samples. The results of this simulation are shown in Figure 16, in which arrows mark the location of observed ^{233}U resonances.

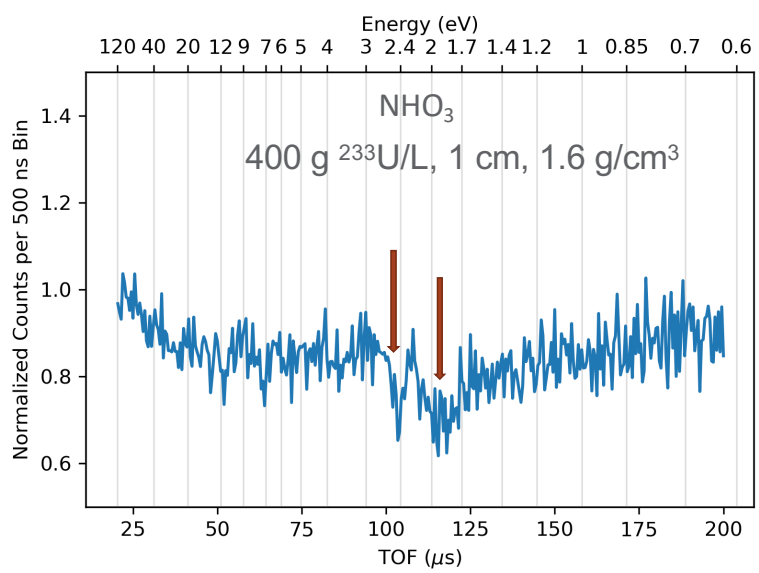

Figure 16. Simulated pNRTA assay result of a 1-cm thick liquid sample consisting of 400 g per liter of ^{233}U. The arrows mark the location of ^{233}U resonances.

4.0 Detector Development

Detectors for pNRTA should have several properties:

1. Short (ideally <100 ns) decay time. Longer decay times may be work if the material has fast rise time (<100 ns) that can be used to accurately measure the detection time. Otherwise, the detector timing may dominate the overall TOF uncertainty.

2. For pNRTA measurements of irradiated samples or in high gamma-ray background environments, gamma-ray sensitivity lower than $1x10^{-8}$, and the ability to discriminate gamma-ray events from neutrons. In lower gamma-ray background environments, such as measurements on fresh fuel, these factors are less important.

3. 'Reasonably good' detection efficiency over the neutron energy range of interest (1-50 eV). Lower efficiencies increase required measurement times to achieve a target assay uncertainty.

4. The detector, its housing, and associated readout components should also have a minimal amount of hydrogenous material to reduce blurring in the TOF spectra from neutron scattering. Note, recent related efforts with pNRTA have successfully used an EJ270 plastic scintillator (Eljen Technologies) (Guembou Shouop and Tshuchiya 2025).

Detectors typically have tradeoffs among these factors. A survey in the first part of the project identified several promising detection approaches. In both modeling studies and measurements, the team explored the following:

- Multi-element (ø25 mm) GS20 detectors for rough pNRTA imaging measurements.
- Tests to compare the gamma-ray sensitivity of He-3 and BCS detectors.
- Designs for a stacked detector BCS system to provide good efficiency and low gamma-ray sensitivity.
- First pNRTA measurements with elpasolite scintillators (CLYC:Ce and CLLBC:Ce). These have longer decay times than GS20, and the ^{6}Li content is lower, but offer excellent gamma-ray/neutron discrimination via pulse shape discrimination (PSD).

The team evaluated these detectors that offer greater gamma/neutron discrimination than GS20 and/or the ability to operate in very high gamma-ray fields, key factors for measuring irradiated samples. For instance, 10 g molten salt samples extracted from the Molten Salt Reactor Experiment created gamma exposure rates around 500 R/hr. Likely higher fields would be expected in measurement scenarios of reactor process lines. There may also be measurement points where fission and activation products are removed prior to measurements (e.g., decay tanks), making scintillator-based detectors practical. All scintillators have gamma-ray sensitivity such that they would likely be overwhelmed by gamma-rays from irradiated material or in high background environments expected in molten salt reactors. However, they may be preferred detection options for unirradiated samples because of their high efficiency and fast timing. We

aimed to demonstrate feasibility of pNRTA across these potential scenarios by finding suitable detectors for each case.

4.1 BCS and He-3 in High Gamma-Ray Backgrounds

Besides fission chambers, which have untenable low detection efficiency for pNRTA, BCS and ^{3}He detectors have among the lowest sensitivity to gamma rays. That is, the number of detected gamma rays that are misclassified as a neutron event divided by the number of incident gamma rays on the detector. This number is dependent on the lower discriminator threshold used by the detector. Gamma-rays produce low-amplitude pulses by depositing a small amount of energy, which can be effectively rejected by raising the discriminator threshold at the cost of also reducing neutron detection efficiency. Recent work by Prof. Angela Di Fulvio showed that a boron-coated straw detector could achieve three orders of magnitude lower gamma-ray efficiencies than typical He-3 detectors, suitable for measurements of neutrons emitted from spent fuel (1e-12) (Fang and Di Fulvio 2023). They conducted measurements with a small neutron source and a gamma-ray source that produced 340 R/hr. Waveforms were digitized from the BCS detector, which allowed thresholds to be adjusted in post-analysis to look at the tradeoff in gamma-ray and neutron efficiencies. Figure 17 shows the intrinsic gamma-ray and intrinsic neutron efficiencies obtained from a ^{252}Cf source vs threshold. The research team at PNNL aimed to reproduce these results with a BCS detector with nearly identical design (just shorter total length). The results below indicate that by simply raising the threshold a great decrease in gamma-ray sensitivity can be achieved with a modest reduction in neutron efficiency.

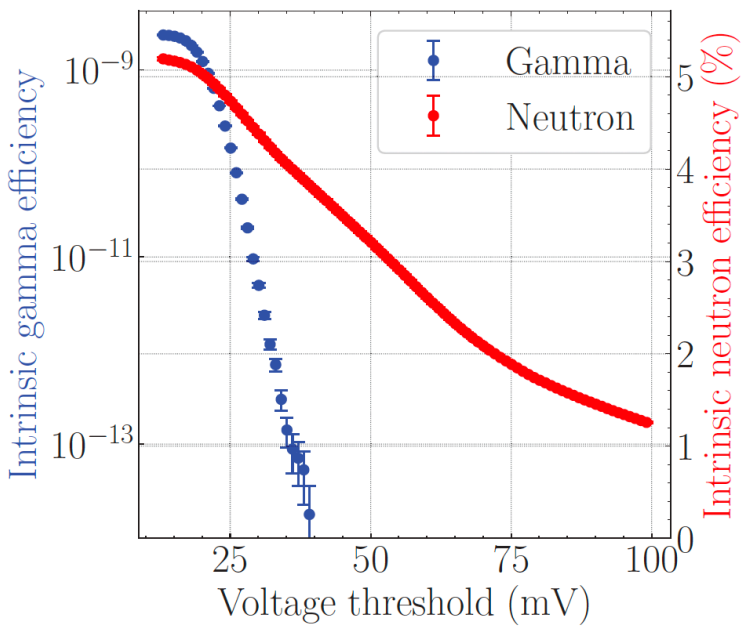

Figure 17. Intrinsic gamma-ray and neutron efficiency as a function of discriminator threshold for a BCS detector [from (Fang and Di Fulvio 2023)].

A prototype BCS detector was acquired from Proportional Technologies, Inc. The design includes seven circular boron coated copper straws enclosed within a tube of ø25.4 mm x 76.2 mm active lengths with an integrated pre-amplifier. The active detection layer consists of 1.3-µm $^{10}B_4C$ layer. A ^{3}He proportional counter with ø25.5 mm x 76.2 mm active length tube with a gas fill pressure of 10 atmospheres was used for comparison measurements.

The experimental setup with both detectors positioned 50 cm away along the source axis to achieve similar exposure rates as the Fang and Di Fulvio experiments. Two small blocks of high-density polyethylene (HDPE) were positioned above and below each detector to moderate neutrons and increase detection efficiency. The analog outputs from each detector were fed into a CAEN DT5730 digitizer to record analog waveforms for post processing analysis. Figure 18 shows the setup at PNNL's High Exposure Facility (HEF), which has large ^{60}Co sources. Table 5 summarizes key detector specifications.

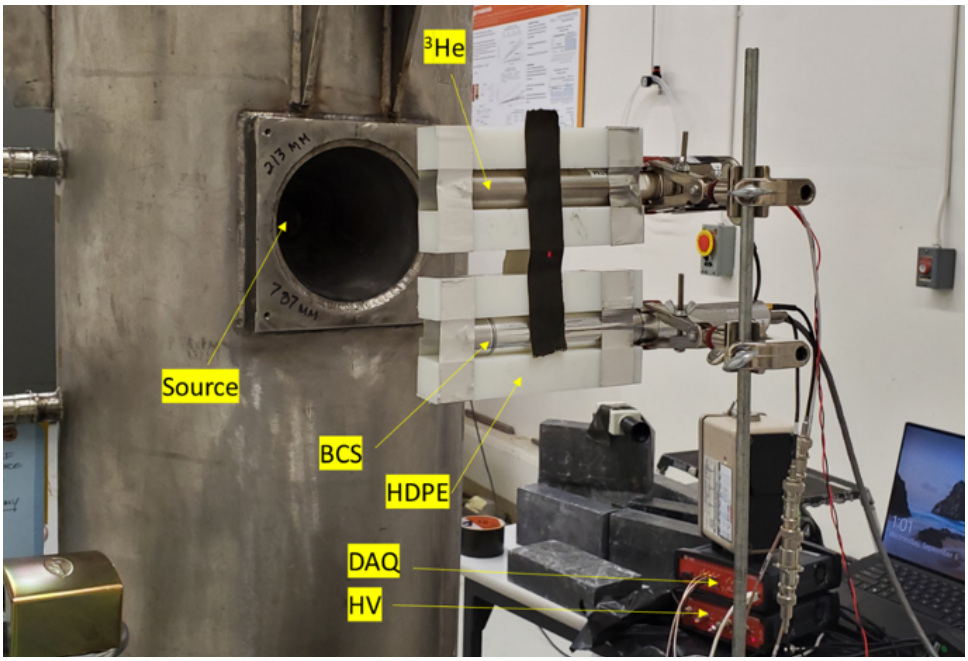

Figure 18. Experimental setup at PNNL's HEF.

Table 5. Detector specifications and parameters.

Parameter	^{3}He	BCS
Active length (mm)	76.2	76.2
Overall diameter (mm)	25.4	25.4
Pressure (atm.)	10.0	1.0
Straw setup	-	ø7 x 7 mm
Straw type	-	Straight tubes

Three separate 10-min measurements were made: neutron-only, gamma-only, and gamma-neutron combined. The neutron measurements were made by placing a ^{252}Cf source directly in between the HDPE block surrounding the detectors. The gamma-only measurements were made using a large ^{60}Co source (375 R/hr.). This was close to the published result, which used a ^{192}Ir source (lower gamma-ray energies). These dose rates were similar to those expected from a 10 g irradiated molten salt sample (500 R/hr). The combined measurements were made in presence of the ^{60}Co and ^{252}Cf sources. Results shown in terms of detector counts versus threshold are shown in Figure 19 show several trends:

- Both detectors see a similar five orders of magnitude decrease in gamma-ray counts as their thresholds are raised
- The ^{3}He is more efficient than the BCS at most threshold values, except above ~12000 ADC units where the BCS is more efficient.
- The drop-off in counts vs. threshold is higher for BCS than ^{3}He.

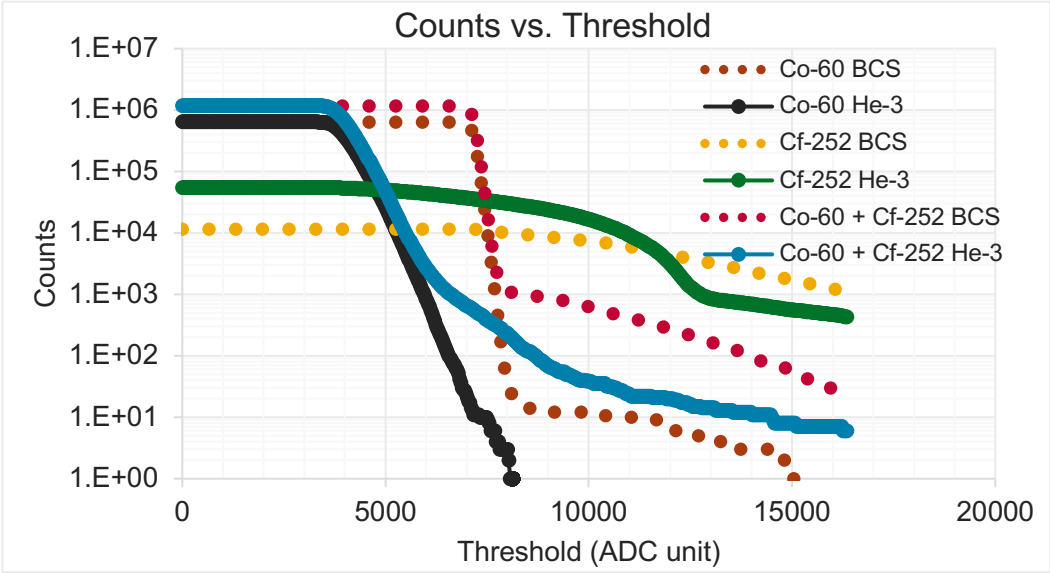

Figure 19. Normalized counts for each detector type as a function of threshold.

Further analysis showed that some of the waveform digitization settings were not optimized, and the BCS straws were round rather than having a pie-shaped cross-sectional area (larger detection area) like the published results. The pie-shaped detectors have up to x3 higher efficiency than the round BCS, and faster charge collection time. We noticed that the waveforms for the BCS almost all had multiple events, making it difficult to accurately count how many gamma-ray and neutrons counts were in the BCS data (Figure 20). Shorter window would increase the counting accuracy. Current analysis counted only the first pulse, so the total counts for BCS at each threshold are significantly underestimated. As such, we expect that BCS will outperform ^{3}He, especially at high thresholds, with the pie-shaped configuration. Further, the high voltage could be adjusted on the detectors to enable a wider dynamic range. Future work would involve repeating measurements with new acquisition settings and computing the intrinsic gamma-ray and neutron efficiencies for fair comparison with the published results.

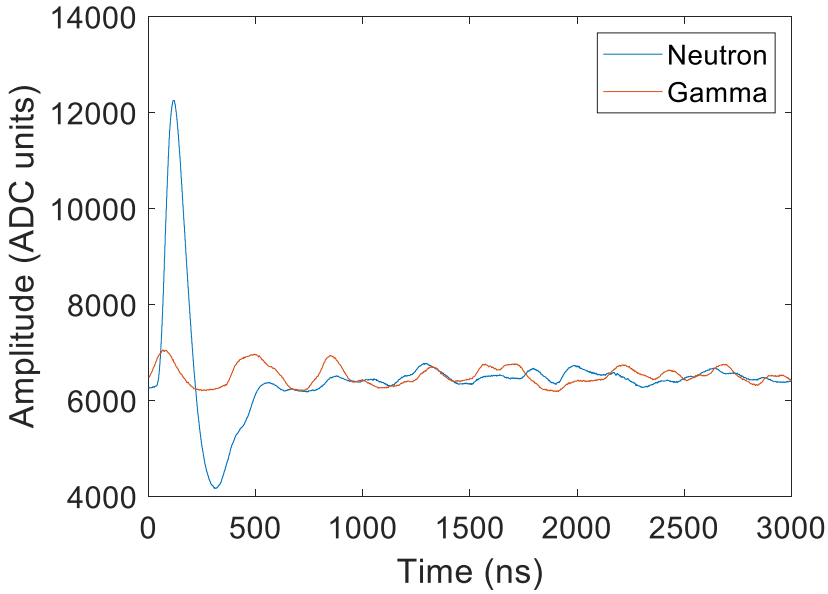

Figure 20. Example analog waveforms for the BCS detector. Note the multiple event pile-up in the gamma waveform.

The single BCS detector was used to collect a TOF spectrum. The low efficiency of the BCS detector meant that no resonances were visible within an hour-long measurement. For BCS detectors to be viable for pNRTA, their overall efficiency must be increased.

4.2 Multi-layered BCS Design

Designs with multi-layer BCS detectors were developed for pNRTA that would provide comparable efficiency to the GS20 and be able to operate in very high gamma-ray backgrounds (Shayaan Subzwari, Rahon, et al. 2024). A key takeaway from this work is that a stack of 15 boron coated straws with internal star configuration (Figure 21) would be as efficient as 5 mm of GS20 for the neutron energies of interest and function in very high gamma-ray backgrounds without grossly misidentifying gamma-rays as neutrons. Such a detector could be likely be assembled from commercial, off-the-shelf detectors and electronics.

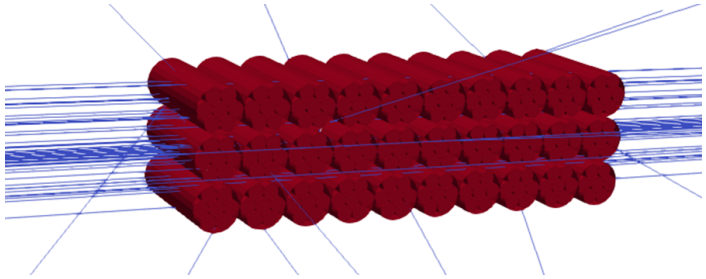

Figure 21. Rendering of stack of BCS detectors simulated in Geant4.

4.3 Elpasolite Scintillators

The team explored how elpasolite scintillator detectors, CLLBC:Ce and CLYC:Ce, would perform compared with GS20. These materials are also sensitive to gamma rays, like GS20, but can separate them from neutrons with high accuracy via pulse shape discrimination. The downsides of this material are that it is slower than GS20 by almost two orders of magnitude (as is BCS) and has less lithium content. These materials may offer improvements over GS20 for samples that are not highly radioactive (and could potentially overwhelm the detector with gamma-ray pileup). An existing benchmarked CLLBC detector model was used that was ø38 x 38 mm^3. This crystal volume has half the amount of Li of the GS20 detector. As such, the detected signal in CLLBC was expected to be lower than the GS20. CLLBC was modeled with four different detector sizes:

- ø38 mm by 38 mm (available size for testing at PNNL)
- ø52 mm by 5.5 mm (similar size as GS20 detector)
- ø52 mm by 42 mm (same diameter as GS20, but longer for equivalent ^{6}Li areal density)
- ø38 mm by 78 mm (available CLLBC diameter, but longer for same Li amount as GS20).

Simulation results are shown in Figure 22. Note the prominent resonances in the CLLBC open beam spectrum compared with GS20, which is nearly free from resonances. The resonances in CLLBC are nearly all from ^{133}Cs (25, 31, and 60 μS, 100% abundance), which overlap with resonances from ^{232}Th and ^{238}U. While a CLLBC detector can achieve comparable signal magnitude as the GS20 with additional crystal depth, CLLBC has prominent inherent resonances that can interfere with those from isotopes of interest (e.g., ^{232}Th and ^{238}U). If the focus of a system is on quantifying ^{233}U or ^{235}U, CLLBC may still be a viable candidate since some of the resonances from those are at lower energies (longer times) and would not be as affected by inherent resonances of the detector material. However, for a system that aims to quantify the amounts of many isotopes in a thorium fuel cycle, the inherent resonances for cesium-containing scintillators may make them an undesirable choice. The pulse shape discrimination is expected to drastically reduce gamma-ray backgrounds compared with GS20. A ø38 x 38 mm^3 CLLBC detector was available for testing at PNNL, but pNRTA measurements were not collected with it pNRTA given initial concerns with its interfering resonances.

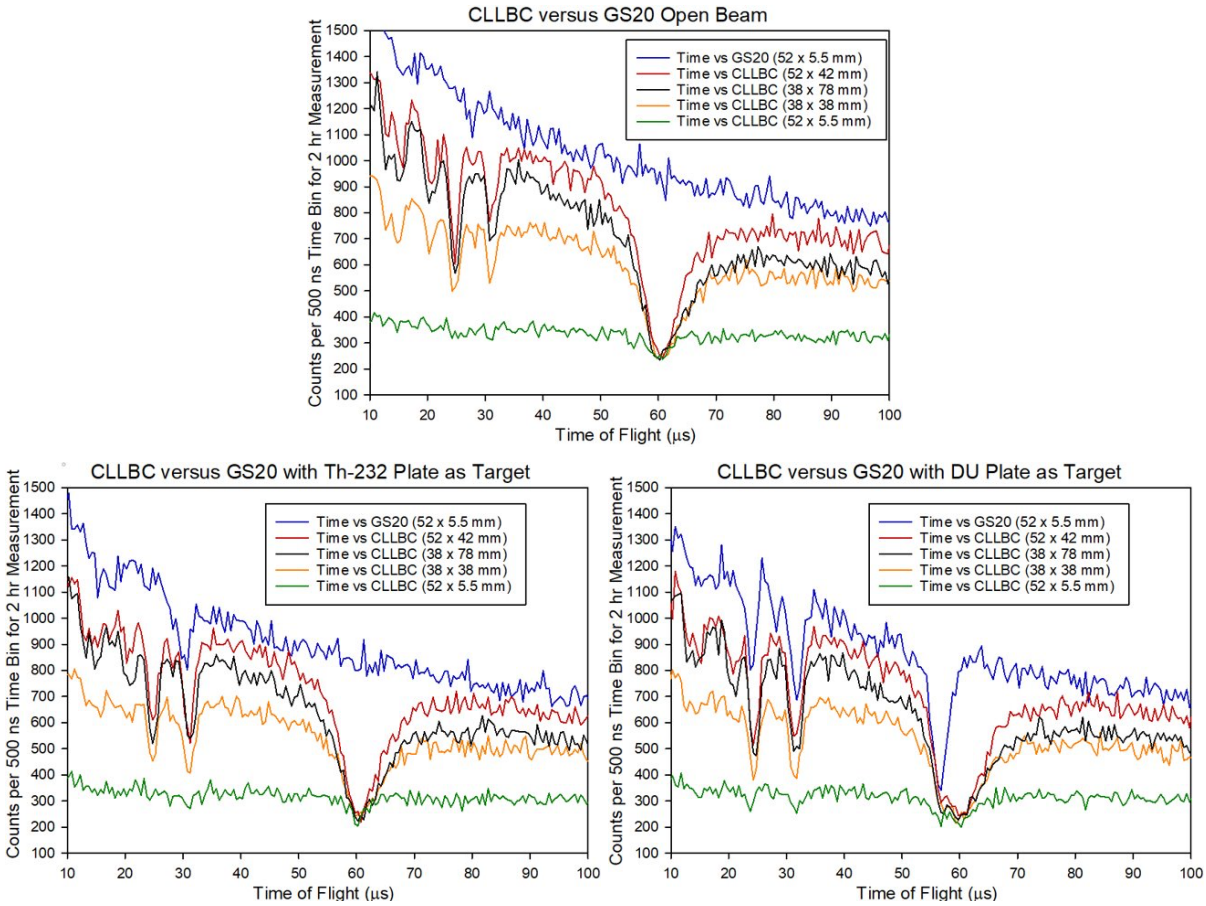

Figure 22. Simulated time of flight spectra for GS20 and CLLBC detectors for open beam (top), ^{232}Th target (bottom left) and DU target (bottom right).

At MIT, further simulations and real measurements were conducted with a CLYC detector (Figure 23). This is detailed in chapter 5 of Subzwari's thesis and summarized here (Shayaan Subzwari 2025).

Figure 23. Photo of a CLYC detector used in pNRTA measurements at MIT.

If the goal of pNRTA measurements is just to assay the fissile isotopes, then the concern about the intrinsic Cs resonances is lessened. This is illustrated in Figure 24, where some of the strongest resonances from ^{233}U and ^{235}U are far from the ^{133}Cs resonances. A 1-cm thick CLYC detector was determined to have efficiency very similar as GS20 and was used for direct

comparison. TOF spectra were collected for both with a 1.5 mm W sheet. Passive data of a ^{232}Th source was also collected for both as an example of elevated gamma-ray background. Both TOF spectra were analyzed with NeuFIT and the W areal density results agreed with each other and within one standard deviation of the true thickness. When the gamma-ray background was added, the CLYC TOF transmission spectrum had noise levels 50% lower than the GS20, a significant improvement. This is shown in Figure 25 below (note the changes in magnitude of the error bars).

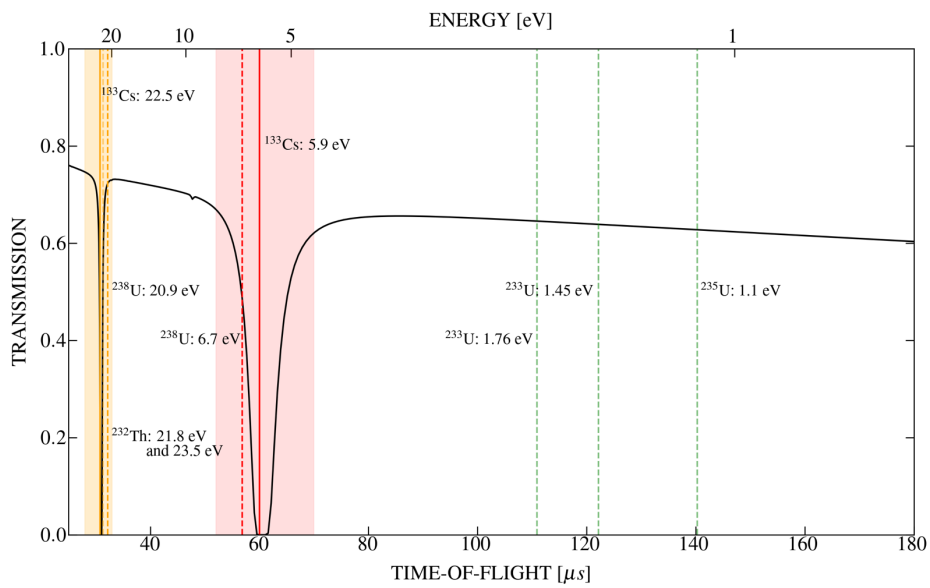

Figure 24. Calculated resonances of ^{133}Cs and vertical lines showing key resonances of safeguards-relevant isotopes.

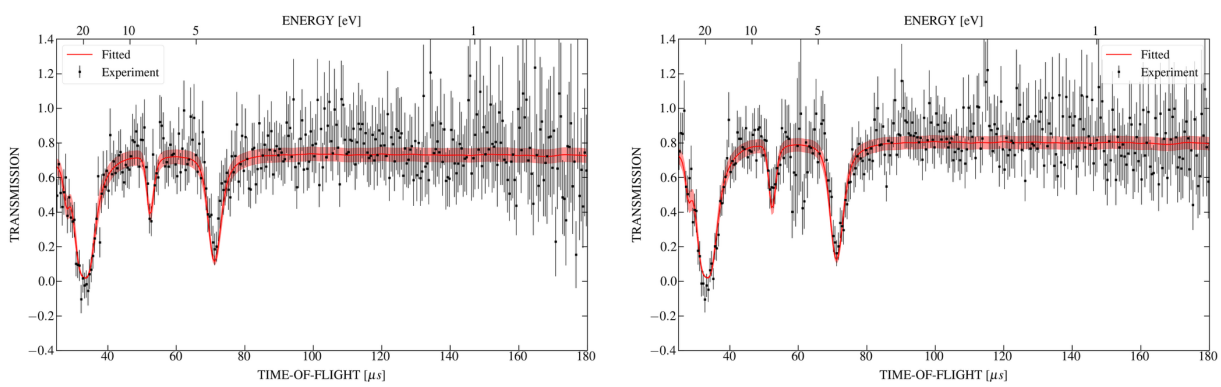

Figure 25. Measured TOF spectra of a 1.5 mm W target with ^{232}Th gamma-ray background included for GS20 (left) and CLYC (right).

4.4 pNRTA Imaging

At MIT, a multi-element GS20 detector was developed and tested. This approach provides spatially resolved assay of target, which can be useful for verifying sample homogeneity. Figure 26 show a schematic of seven detectors inside a cylindrical shield at MIT.

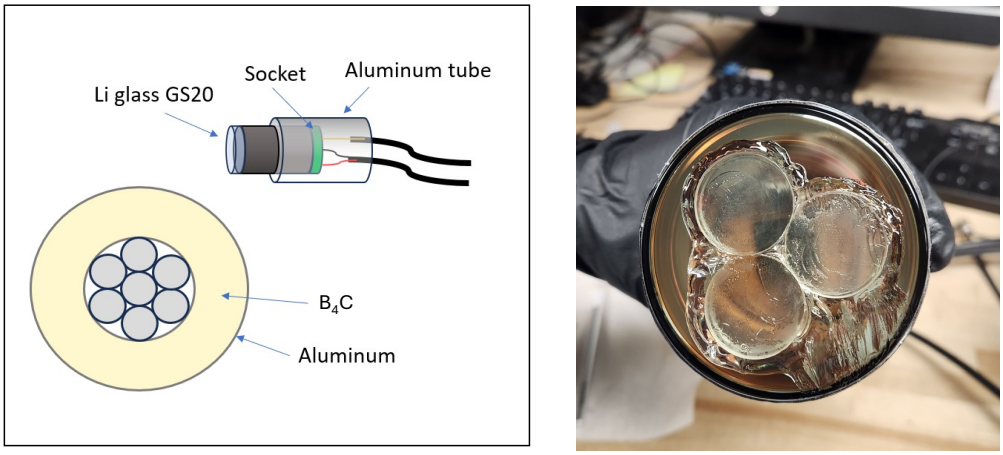

Figure 26. Schematic (left) and photo (right) of a multi-element GS20 detector tested at MIT.

Photographs of a test setup at MIT are shown in Figure 27, including targets of Ta and W (left) and two detectors behind the separate targets (right). Because of the separate alignments of the targets and detectors, it is expected that the TOF spectra will show the distinct resonance from each target in the different detector channels.

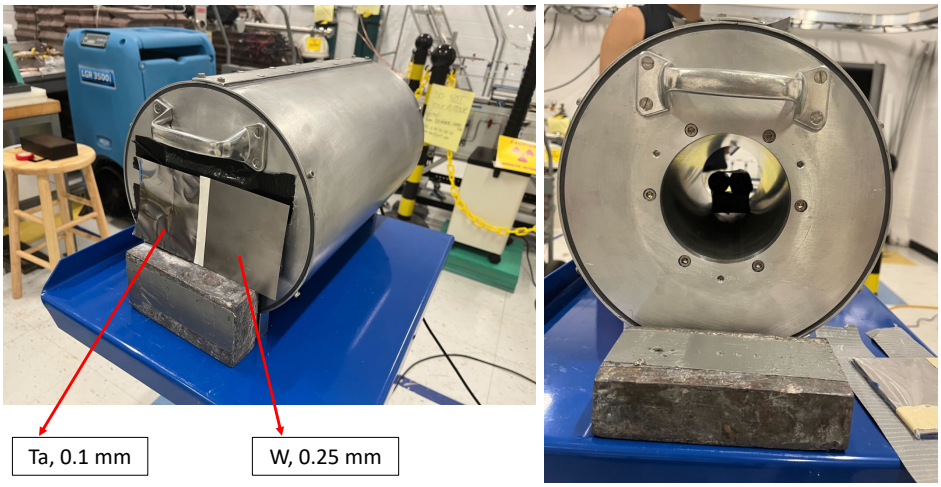

Figure 27. Photographs of the NRTA targets (Ta and W plate), cylindrical neutron shield, and GS20 detectors within the shield at MIT.

As expected, initial analysis shows that the key resonances from Ta and W are visible in the TOF spectra (Figure 28). In the spectra, only the resonances with the highest cross-sections are readily visible. This illustrates that the basic feasibility of using segmented detectors is feasible with the pNRTA setup in reasonable measurement times (30 min). Another test showed open beam and 1 mm W plate TOF spectra for both detectors, showing similar responses for both detectors (Figure 29).

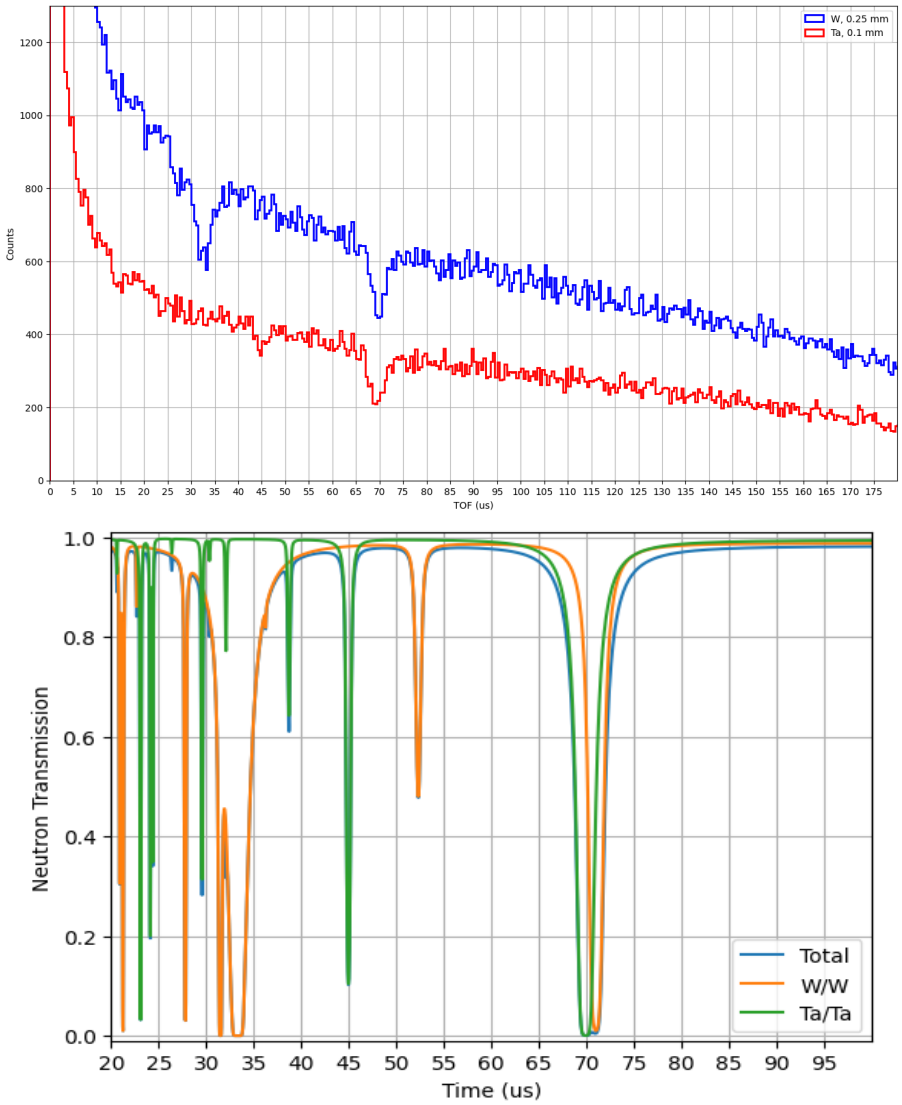

Figure 28. (Top): Measured TOF spectra for the two detectors, showing the strongest resonances for W (blue) and Ta (red) for a 30-min test run. (Bottom): Calculated neutron transmission showing saturated resonances at ~70 and 20-35 μS.

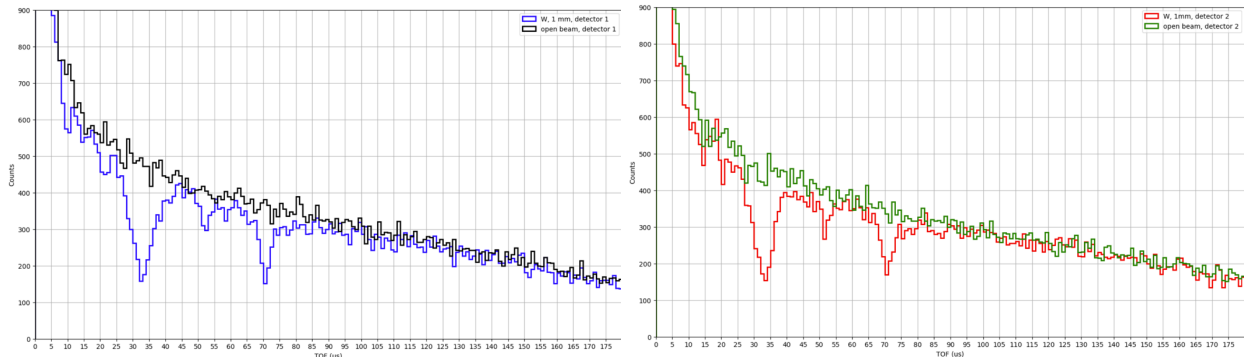

Figure 29. Open beam and 1 mm W plate TOF spectra for detectors 1 (left) and 2 (right).

4.5 Detector Study Summary

A stop light chart (green good, yellow moderate, red poor) that shows detector strengths and weaknesses for pNRTA criteria is shown in Table 6. Timing refers to the detector decay time (faster is better). Gamma-ray sensitivity ("Gam. Sens.") should be minimal, and neutron efficiency ("Neu Eff") should be high. Neutron/gamma-ray discrimination should also be high ("N/G disc."). Further, the intrinsic detector materials should not have major interfering neutron resonances in the energy range of interest ("Intrin. Reso.").

No detector meets all criteria. Improvements to a BCS detector design offer straightforward ways to increase neutron efficiency. This includes using pie cross section detectors, stacking multiple detector tubes. The main drawback of this approach is an increase in readout channels. Another promising detector option discovered near the end of the project is scintillating Nanoguide (Incom, Inc.) (Myllenbeck et al. 2021). It consists of a glass of polystyrene base with boron- or lithium-loaded organic glass scintillator and has been tested in related neutron resonance imaging experiments (Wolfertz et al. 2024). An Anger-camera design with Nanoguide could offer a way to make adjustable-resolution imaging measurements (from single pixel to higher spatial resolution if measurement time permits).

Table 6. Stoplight chart for the detector comparison study.

Detector	Timing	Gam. Sens.	Neu. Eff.	N/G Disc.	Intrin. Reso.
GS20					
^{3}He					
BCS					
Stacked BCS					
CLLBC/CLYC					
Nanoguide					?

5.0 Measurements & Analysis

5.1 Samples

A set of relevant samples or prepared for pNRTA measurements (Table 7).

Table 7. Description of samples/targets used in pNRTA experiments at PNNL.

Target	Photo
3-mm thick ^{232}Th metal Isotrak Source (Isotope Products) 0.25 mm steel enclosure, 11.7 g/cm^3	
High-Assay Low-Enriched Uranium mini-plates, U10Mo, 0.635 mm thick, 17.2 g/cm^3, ~3 g ^{235}U per plate. Two-deep and three-across taped to Al backing plate	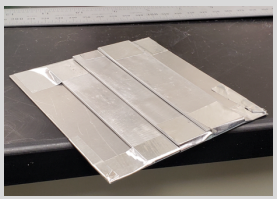
Two custom ^{233}U oxide powder samples, 1.2 mm thick, tap density 1.56 g/cm^3, 0.689 uranium fraction, 98.2% ^{233}U, aluminum holder, RMT 125768 (3.52 g of UO_2) and RMT 124319 (	
Bare depleted uranium metal plate in aluminized Mylar bag, (0.22 wt.% ^{235}U) metal plate, 15.2×15.2×3.0 cm^3, RMT 11138	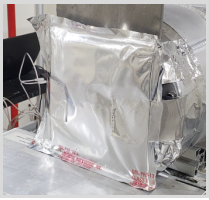
Highly enriched uranium metal plate in a polycarbonate container (91.28 wt.% ^{235}U (103 g U), ~ø23 x 0.13 cm^3, RMT 41762	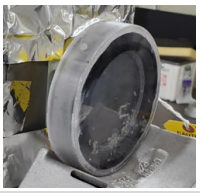
Non-radioactive foils/plates such as tungsten and indium for testing, determining backgrounds, etc.	

These samples were measured in individual and stacked configurations to create different areal densities of nuclear materials in the path of the neutrons.

5.2 Example Measurement Configurations

Since the mid-project report, several measurement campaigns were conducted. Primarily, these consisted of stacking samples and incorporating HALEU targets. This section describes some of the configurations. Two ^{233}U oxide powder samples were prepared in custom sealed container for pNRTA measurements as described in (B. McDonald, Burnett, Clark, Danagoulian, Gilbert, Klein, et al. 2022). A third container "blank" was loaded with CeO_2. An example of a measurement set up with one target is shown in Figure 30. For a given setup, the open beam measurement included any non-target materials such as lead shielding. Figure 31 shows an example stacked target configuration with ^{233}U, ^{232}Th, and 25 mm of lead to shield the GS20 detector for the large number of gamma-rays from ^{233}U.

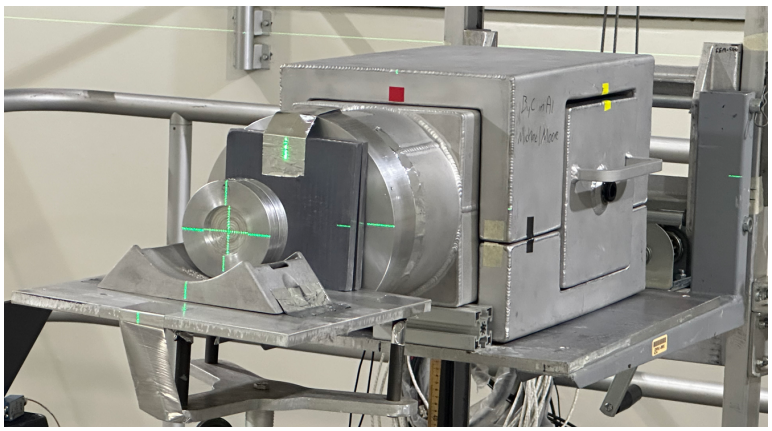

Figure 30. Photo of a ^{233}U oxide target with lead plates to reduce gamma-ray signal in the GS20 detector (inside the boron carbide shield). A laser level was used to align the DT generator, targets, and detector.

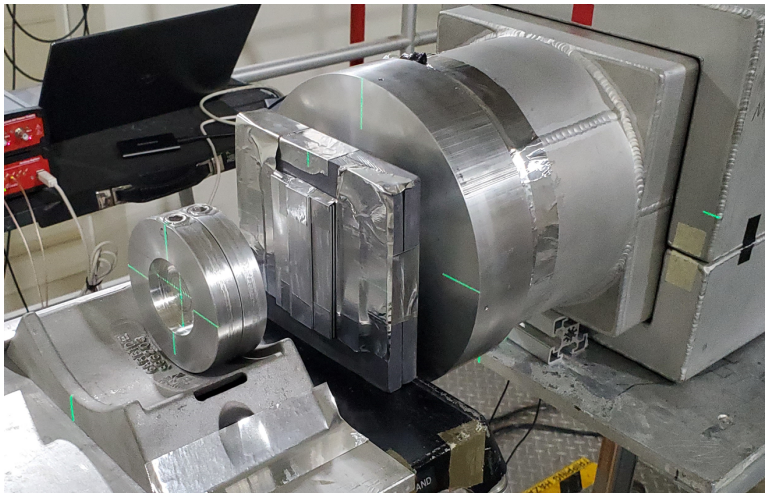

Figure 31. Photo of a stacked target configuration with two ^{233}U oxide sources, six HALEU mini-plates, and 25 mm of lead.

5.3 Outdoor Measurements

As part of her dissertation work, MIT graduate student LTC Jill Rahon performed outdoor measurements with a P383 DT neutron generator and compared backgrounds with indoor measurements at PNNL and MIT. Background levels were significantly lower outdoors than both indoors measurements. PNNL's low scatter facility oddly had higher background rates for many neutron TOF energies than the MIT vault (Figure 32).

Dose measurements were also made around the neutron generator. As one example, The H*(10) dose rate for an operator was measured at 5 m with no shield around the neutron generator to be 5 mrem/hr (neutron) and ~1 μrem/hr (photon). She also modeled the concept of performing NRTA/NCRA measurements in the back of a truck. These results add credibility for the potential use of these techniques in field measurements.

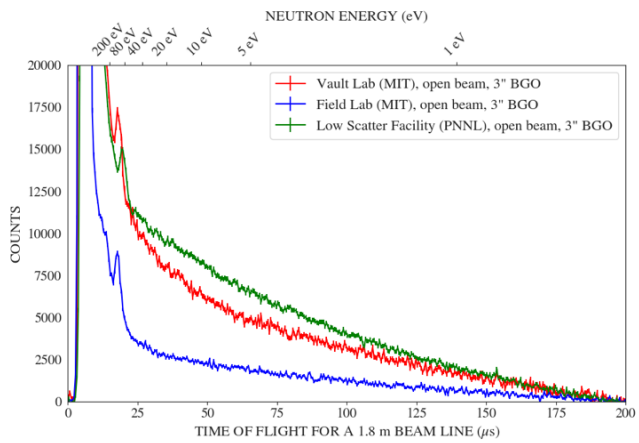

Figure 32. TOF spectra for a 1.8 standoff in three different locations (Rahon 2024).

5.4 Analysis Process

Background in pNRTA measurements comes from several different sources. A background model was developed to account for (i) off-axis room background (constant), (ii) on-axis target-dependent background (var), and (iii) passive background from the target's inherent radioactivity (pass):

$$C_{bg}^{tot} = C_{const} + e^{-n \cdot \sigma_{tot}(E^{offres}) \cdot x} \cdot C_{var} + C_{pass}$$

Where the second term is the target-dependent background, n is atomic density, $\sigma_{tot}(E^{offres})$ is the total neutron cross-section at off-resonance epithermal neutron energy, and x is the target thickness. These contributions were determined empirically using a set of thin- and thick-resonant targets (e.g., W, Ag, and In targets along with open beam and an off-axis measurement with the collimator is plugged with boron carbide) to determine the different background contributions (Benjamin S McDonald et al. 2024; E.A. Klein 2023). As discussed in the first reference, the ø42 mm collimator developed in this effort reduced the on-axis (target-dependent) background by ~70% for the ^{232}Th target, indicating that this component was smaller than off-axis (shield-penetrating) neutron background.

The experimental transmission was calculated by correcting the target-in and target-out spectra for background and taking their ratio:

$$T_{expt} = \frac{C_{in} - C_{bg,in}}{C_{out} - C_{bg,out}}$$

The experimental transmission can then be compared with MCNP results, or results from a calculated forward model. Often a quick comparison was made to calculated transmission spectra based on ENDF-B/VIII.0 neutron cross sections (i.e., as performed by the iNEUIT program) convolved with a system resolution function. The resolution function accounts for uncertainty in the neutron time-of-flight due to the finite nature of the source neutron pulse width and the distribution in neutron moderation time. The resolution function can be approximated by a Gaussian with width σ_{res} which was empirically determined to be approximately $0.8\ \mu s$.

$$T_{calc} = e^{-n \cdot \sigma_{tot}(E) \cdot x} * \mathcal{N}(0, \sigma_{res})$$

6.0 Algorithm Development & Assay Results

In the first year of the project, the team developed an algorithm to estimate isotopic areal densities from TOF data. The inverse problem approach worked well for simple samples. When sample complexity increased, such as by stacking multiple targets with overlapping resonances or creating less (i.e., noisier) transmission, the algorithm struggled to produce accurate results. We next turned to REFIT-2009, the gold standard code used for NRTA (Moxon, Ware, and Dean 2010). Table 8 contains some of key distinguishing resonances for the key isotopes targeted in this project (Benjamin S McDonald et al. 2024).

Table 8. Example target resonances for isotopes of interest and peak total cross sections.

Target	Resonance Energy	Σ Peak
[-]	[eV]	[b]
Th-232	21.8	1824
Th-232	23.5	2628
U-233	1.7	1054
U-233	2.3	1037
U-233	10.4	660
U-234	5.2	16366
U-235	6.38	540
U-235	8.76	925
U-235	19.35	1085
U-238	6.67	7229
U-238	20.9	9430

Figure 33 contains TOF spectra that were analyzed with REFIT for different targets, with prominent resonances visible from all but ^{233}U (not included). In this case, the nearby resonances of ^{232}Th were distinguishable.

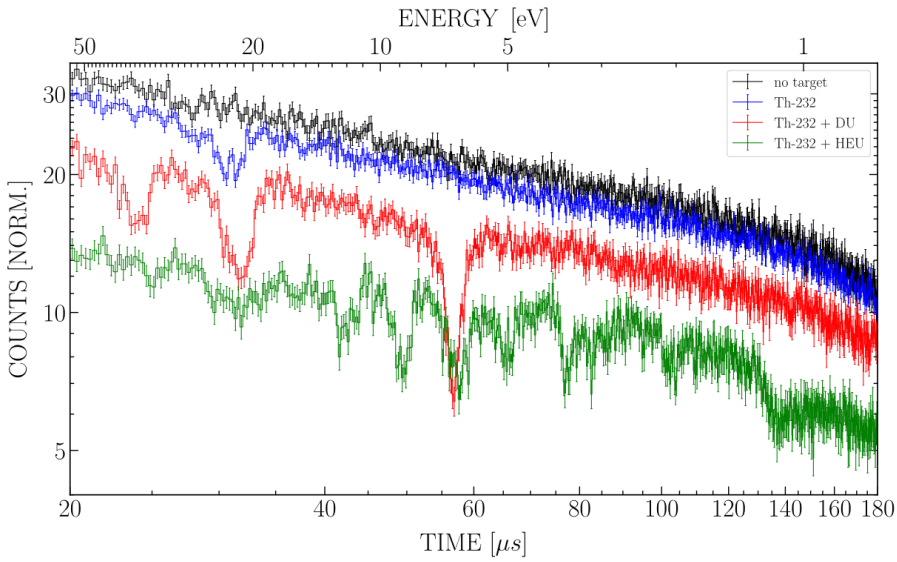

Figure 33. TOF spectra of four different target configurations (E.A. Klein 2023).

6.1 REFIT-2009

First measured TOF spectra ^{233}U and ^{232}Th targets analyzed with REFIT were encouraging. The predicted mass of ^{233}U was 2.7 $\pm$0.5 g, within one standard deviation of the estimated true value of 2.5 $\pm$ 0.25 g. This indicated that ^{233}U mass can be detected and quantified at gram levels within 2-hour measurement times with pNRTA. The fitting results from REFIT and the measured TOF spectrum are shown in Figure 34.

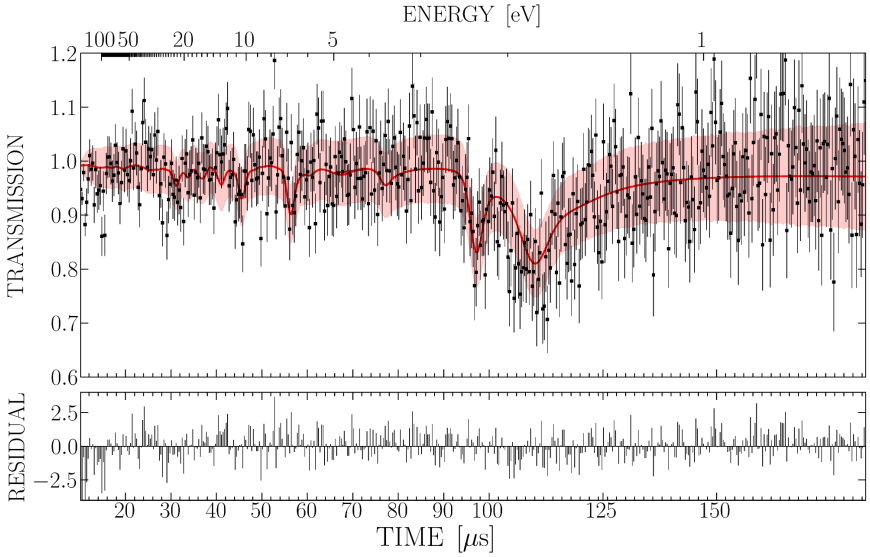

Figure 34. Measured (black) and REFIT (red) TOF transmission spectrum from ^{233}U oxide target. Residuals are numbers of standard deviations.

Subsequent measurements included stacked configurations and combinations of the Table 7. Data was processed with REFIT, and the results are summarized in Table 9. The first three rows are repeat measurements of the ^{232}Th target taken several months apart. This shows a

measure of repeat assay uncertainty, including the effects of system assembly/disassembly. For these measurements the mean bias and RSD were 27.5% and 9.8% respectively.

REFIT requires an initial estimate for the isotopes within the sample and their concentrations. For each sample with uranium (all but the ^{232}Th only samples), equal weighting was given for all the uranium isotopes to avoid biasing the results. REFIT performed the best for samples with just one dominant isotope (e.g., ^{232}Th, ^{233}U). When ^{232}Th was combined with HEU or DU targets, the ^{232}Th and ^{235}U/^{238}U resonances partially overlapped, leading to a reduction in the ^{232}Th estimates. ^{232}Th underestimated in presence of HEU and DU (overlapping resonances). All isotopes were estimated to within roughly an order of magnitude, and the ^{233}U was estimated to better than 10%. REFIT uncertainties scaled proportionally with the isotopic concentration (e.g., large uncertainties for ^{234}U and ^{236}U)

Table 9. REFIT results of sample configurations measured at PNNL (E.A. Klein 2023).

Sample	Meas. Time (min)	Isotope	Predicted Abund. (at/b)	True Abund. (at/b)
Th	60	^{232}Th	$(1.06 \pm 0.04) \times 10^{-2}$	0.91×10^{-2}
Th	60	^{232}Th	$(1.19 \pm 0.03) \times 10^{-2}$	
Th	60	^{232}Th	$(1.23 \pm 0.04) \times 10^{-2}$	
Th + DU	120	^{232}Th	$(7 \pm 2) \times 10^{-3}$	0.91×10^{-2}
Th + DU	120	^{235}U	$(6 \pm 5) \times 10^{-5}$	3.6×10^{-5}
Th + DU	120	^{238}U	$(1.04 \pm 0.04) \times 10^{-2}$	1.4×10^{-2}
Th + HEU	120	^{232}Th	$(4 \pm 1) \times 10^{-3}$	0.91×10^{-2}
Th + HEU	120	^{234}U	$(4 \pm 1) \times 10^{-5}$	4.7×10^{-4}
Th + HEU	120	^{235}U	$(6.4 \pm 0.2) \times 10^{-3}$	3.89×10^{-3}
Th + HEU	120	^{236}U	$(2 \pm 13) \times 10^{-6}$	1.9×10^{-5}
Th + HEU	120	^{238}U	$(2.8 \pm 0.7) \times 10^{-4}$	2.2×10^{-4}
$^{233}UO_2$	150	^{233}U	$(3.5 \pm 0.6) \times 10^{-4}$	$(3.3 \pm 0.1) \times 10^{-4}$

The next step was to measure targets with ^{233}U and ^{235}U, since quantifying these isotopes when present together is a prime goal. We expect that these isotopes will not have the same issue as ^{232}Th when combined with ^{235}U because ^{233}U has distinct resonances apart from ^{235}U near 1-2 eV. These data were acquired but not analyzed with REFIT.

6.2 NeuFIT

A weighted least squares program was developed to fit expected transmission curves to experimental transmission spectra that aimed to be open source, comprehendible (REFIT source code is not accessible). This was a main thrust of MIT graduate student, Shayaan Subzwari's, master's thesis (Shayaan Subzwari 2025). Figure shows results for configurations with Th-232 and U-233. Figure 2 shows experimental and fitting results for configurations with HALEU and/or U-233. In general, the fitting program matches experimental data quite well. Isotopic concentration results are provided in Table 1.

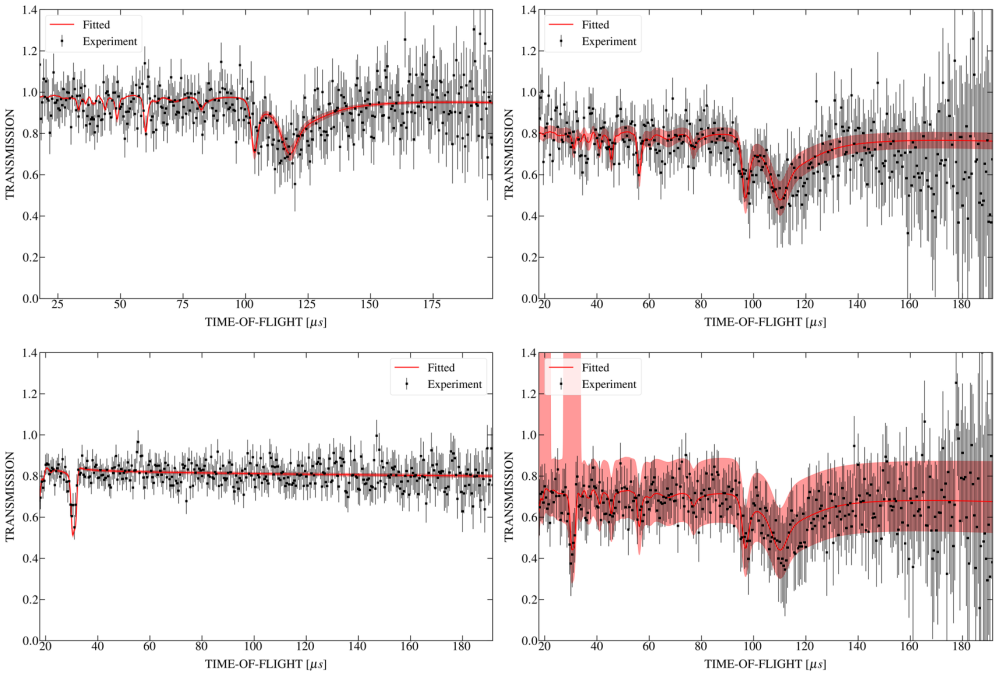

Figure 35. Experimental and NeuFIT TOF spectra for different targets. (Top left): One ^{233}U target. (Top right): Two stacked ^{233}U targets (each with similar areal density). (Bottom left): ^{232}Th target. (Bottom right): ^{233}U targets stacked with ^{232}Th target.

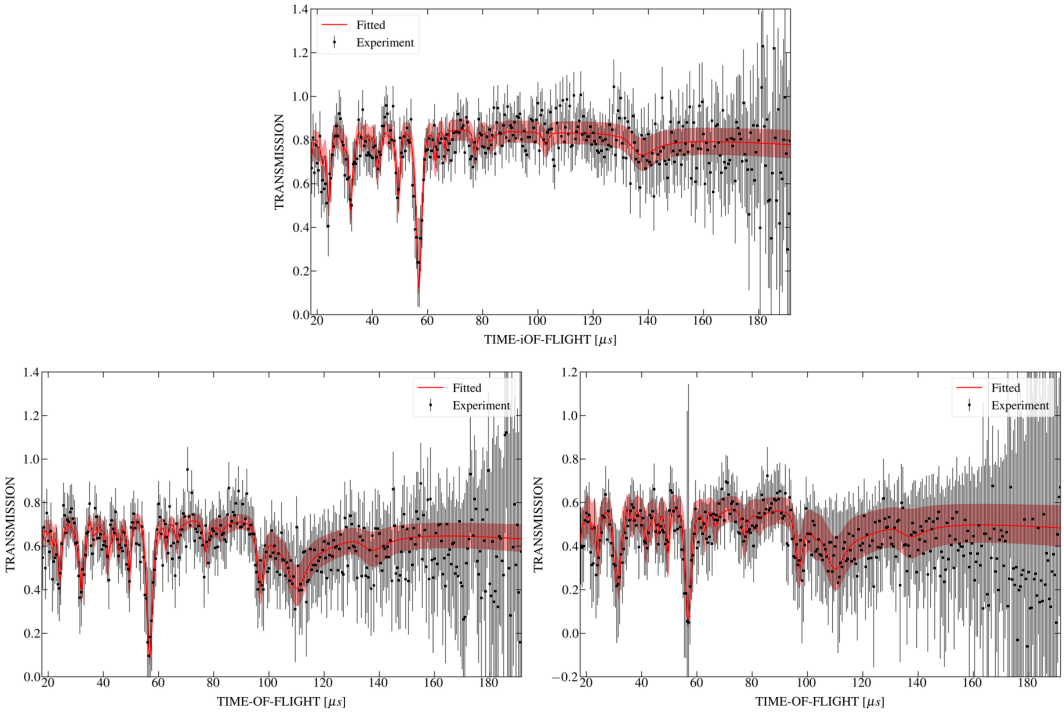

Figure 36. Experimental and NeuFIT TOF spectra for different targets. (Top): HALEU mini plates. (Bottom left): Mini plates stacked with both ^{233}U samples. (Bottom right): Mini plates stacked with ^{233}U samples and ^{232}Th plate.

Table 10. Summary of NeuFIT assay results for PNNL target configurations. Uncertainties in the 'true' values for the 233U samples were estimated to be ~10%. Z = (predicted-true)/(predicted error), is a measure of the prediction error relative to the predicted value.

Target	Time (min)	Isotope	Predicted Abund. (at/b)	True Abund. (at/b)	% Diff	Z
Th	120	232Th	$1.12 \pm 0.03 \times 10^{-2}$	0.91×10^{-2}	23.1%	7.0
UO_2, sample 1	150	233U	$2.55 \pm 0.37 \times 10^{-4}$	$3.22 \pm 0.36 \times 10^{-4}$	-20.8%	-1.8
UO_2, sample 2	180	233U	$2.89 \pm 0.42 \times 10^{-4}$	$3.10 \pm 0.34 \times 10^{-4}$	-6.8%	-0.5
Both UO_2, samples	180	233U	$4.81 \pm 0.54 \times 10^{-4}$	$6.32 \pm 0.50 \times 10^{-4}$	-23.9%	-2.8
Th + UO_2 samples	180	232Th 233U	$1.97 \pm 0.71 \times 10^{-2}$ $4.47 \pm 0.54 \times 10^{-4}$	0.91×10^{-2} $6.32 \pm 0.5 \times 10^{-4}$	116.5% -29.3%	1.5 -3.4
HALEU	180	235U 238U	$1.39 \pm 0.28 \times 10^{-3}$ $5.59 \pm 1.11 \times 10^{-3}$	1.44×10^{-3} 5.73×10^{-3}	-3.5% -2.4%	-0.2 -0.1
UO_2 samples + HALEU	180	233U 235U 238U	$5.02 \pm 0.59 \times 10^{-4}$ $1.40 \pm 0.39 \times 10^{-3}$ $7.09 \pm 1.98 \times 10^{-3}$	$6.32 \pm 0.5 \times 10^{-4}$ 1.44×10^{-3} 5.73×10^{-3}	-20.6% -2.8% 23.7%	-2.2 -0.1 0.7
Th + UO_2 samples + HALEU	180	232Th 233U 235U 238U	$1.29 \pm 1.13 \times 10^{-2}$ $6.05 \pm 0.74 \times 10^{-4}$ $1.69 \pm 0.55 \times 10^{-3}$ $7.50 \pm 2.42 \times 10^{-3}$	0.91×10^{-2} $6.32 \pm 0.50 \times 10^{-4}$ 1.44×10^{-3} 5.73×10^{-3}	41.8% -4.3% 17.4% 30.9%	0.3 -0.4 -0.4 0.7

Key takeaways include:

- As the number and complexity of stacked targets increases, the uncertainty in the results also increases. This follows because fewer neutrons pass through thicker samples, creating greater statistical uncertainty. Further, some isotopes have some overlapping resonances, which may cause the fitting program to incorrectly estimate abundances (e.g., ^{232}Th and ^{238}U within 1 eV).

- As the ^{233}U abundance in the beam was doubled, the transmission halved as expected. The predicted ^{233}U abundance for the stacked ^{233}U targets was roughly double that of the single ^{233}U targets.

- The abundances for all the targets are reasonably consistent across the various experiments (and with the previous data runs, as well).

- For all samples, the computed mean bias and relative standard deviations were 9.3% and 36.5%, respectively. If the ^{232}Th outlier of 116.5% is removed (further investigation is warranted), these values drop to 1.5% and 21.4%.

- This dataset shows that it is possible to estimate the isotopic abundances of ^{233}U, ^{235}U, and ^{238}U in these configurations with a pNRTA prototype with better than 30% accuracy.

Preliminary comparison of REFIT-2009 and NeuFIT shows that uncertainties and accuracies are similar, agreeing within two standard deviations. New Fit showed a negative bias for the U-233 sample compared with REFIT. Currently NeuFIT used the entire time-of-flight spectrum,

which is likely not optimal since the main information content for ^{233}U is around 100-120 μs. At longer times, the data is noisier, and at shorter times, the energy resolution is poorer. REFIT-2009 uses specified regions of interest for on- and off-resonance regions which must be chosen.

6.3 Current Limitations

Though the assay results have overall showed feasibility of pNRTA for quantitatively measuring relevant samples for thorium fuel cycle safeguards, several limitations of the technique were also discovered through the course of the project. These include potential interferences from other, non-actinide isotopes that may be present in a sample or detector, longer-than-desired measurement times, the impact of high radioactive samples or environments on detector performance, and decreasing assay performance with sample complexity (i.e., number of isotopes and increasing areal density).

pNRTA can assay samples in containers of many materials. Lead moderately attenuates epithermal neutrons but has no resonances from 1-100 eV. Iron and aluminum similarly do not have any energy-dependent features over this range. Nickel, the main element in Hastelloy-N, a special corrosion-resistant material developed for molten salt reactors, has no resonances, but is highly attenuating. Measurements and simulations showed a ~70% reduction of transmitted neutrons with 9 mm of Hastelloy-N. Resonances are still discernable with such shielding, but less prominent, likely degrading assay precision. Measurements with the ^{233}U samples included up to 25 mm of lead. These measurements took longer to acquire adequate statistics, but the isotopic concentration was still quantifiable. Nearly all mid- and high-Z isotopes have some resonances below 100 eV, many have resonances < 10 eV (Postma and Schillebeeckx 2017). These can possibly interfere with assay of safeguards isotopes of interest, so it is important to know approximately what is in the sample rather than assuming it could be anything within the chart of the nuclides.

Measurement times of up to three hours may be acceptable for some scenarios but should ideally be reduced so more samples can be measured in each shift. There are several ways to reduce measurement time:

- Increase detector efficiency and area (latter typically also means increasing sample area). CLYC and BCS detectors offer two options for increasing efficiency without adding to gamma-ray backgrounds.

- Reduce flight path to improve $1/r^2$ geometric efficiency. This trades efficiency for TOF resolution. It may be possible to sacrifice some of the latter for a system focused on assay of ^{233}U and ^{235}U.

- Incorporate sources with higher neutron yield

Sample temperature can also impact the width of resonances, which could impact assay performance depending on whether the analysis algorithm is sensitive to these changes (Lan et al. 2024). Further investigation is warranted with simulated TOF spectra corresponding to measurements at different sample temperatures relevant to molten salt reactors.

Low concentrations of ^{233}U and other isotopes used in some fuel types may be below the sensitivity limit of the current prototype. pNRTA modeling of MSRE fuel targets did not show

resonances from ^{233}U, but a fuel with an order of magnitude higher concentration of ^{233}U did produce resonances.

7.0 Conclusions & Future Directions

The modeling, experiments, and analysis results in this project demonstrate that pNRTA is feasible for assaying ^{232}Th, ^{233}U, ^{235}U, and other isotopes in many forms, including metals, ceramics, salts, and even liquids. A summary of assessed samples is given in Table 11. The pNRTA prototype shows significant promise as a new capability for non-destructive assay (NDA) for thorium fuel cycle safeguards. This level of precision for assaying gram-level samples with ^{233}U and ^{235}U does not currently appear achievable with other NDA methods.

Table 11. Sample forms and compositions either measured or simulated in the project.

Target	Meas. Time (min)	Isotopes	Accessible with pNRTA?
^{233}U oxide (1.2 mm)	150	^{233}U	Yes
^{232}Th metal (3 mm)	60	^{232}Th	Yes
^{232}Th + DU metal	120	^{232}Th/^{235}U/^{238}U	Yes
^{232}Th + HEU metal	120	^{232}Th/^{234}U-^{238}U	Yes
^{233}U + HALEU (0.6 mm)	180	^{233}U-^{238}U	Yes
^{233}U + HALEU + ^{232}Th	180	^{232}Th/^{233}U-^{238}U	Yes
Simulated Shippingport Reactor Fuel Pellets (Taylor and Loo 1999)	60	^{233}U, ^{232}Th	Yes
Simulated Molten Salt Reactor Fuel, 0.137 mol % $^{233}UF_4$, 3- 10 mm (Houtzeel and Dyer 1972)	60	^{233}U, ^{232}Th	No, low U concentration
Simulated Molten Salt Fast Reactor Fuel, 2.5 mol % $^{233}UF_4$, 10 mm (Heuer et al. 2014)	60	^{233}U, ^{232}Th	Yes
High U concentration acid (400 g ^{233}U/L) (10 mm)	60	^{233}U	Yes

Key project outcomes:

Modeling & Simulation: A high-fidelity MCNP model was developed, refined, and benchmarked with experimental data. It was used to simulate TOF spectra for a range of targets relevant to thorium fuel cycle safeguards and conduct sample parameter studies. Assessed pNRTA's ability to measure a range of different MSR compositions and sizes.

Detector Study: A detector evaluation study identified promising alternative detectors to GS20 for irradiated and non-irradiated samples. Initial measurements with CLYC showed improved uncertainty in TOF spectra compared with GS20 for samples with higher radioactivity thanks to CLYC's far superior neutron/gamma discrimination capability. Irradiated samples will require a neutron detector with very low gamma-ray sensitivity and accurate neutron/gamma-ray discrimination. The most promising detectors identified for this purpose were ^{3}He and stacked BCS. A multi-element stacked BCS detector was designed and determined via simulations to have similar efficiency as 5 mm of GS20. BCS and ^{3}He detectors were assessed in high gamma fields expected from irradiated samples.

Measurements & Analysis: The team measured and analyzed unique data set of U/Th targets in different configurations, including the first ever pNRTA measurements of ^{233}U and HALEU. REFIT was used to analyze experimental and simulated TOF spectra. Assay precision decreased proportionally with sample radioactivity with the GS20 detector due to increased gamma-ray backgrounds. This was most evident with the ^{233}U samples, which required up to 25 mm of lead shielding and decreased the neutron signal. Repeat measurement uncertainty over several months for one sample was ~10%. A custom, open-source analysis algorithm (NeuFIT) was developed, which showed similar performance as REFIT with understanding of how the program works. For the set of 15 isotope assays (from measurements of eight targets), the mean bias and RSD were 9 and 36%, respectively.

Several important areas of future research were identified in this effort:

Neutron Source: Explore different neutron source options that could potentially increase TOF resolution (e.g., dense plasma focus sources), reduce measurement times (e.g., with higher neutron yield or with forward-directed emissions), or improve system practicality (e.g., use DD instead of DT source). Future work could design neutron source shield that doubles as an epithermal neutron moderator to reduce dose rates to below levels of regulatory control while keeping the spread of moderation times small.

Algorithms: Currently NeuFIT uses the entire TOF spectrum to estimate isotope concentrations. At the earlier times the resolution is poorer, and at the longer times the uncertainties become larger. Depending on the target assay isotopes, a tailored approach where only part of the spectra is analyzed may improve overall assay performance and robustness to interferences. It may also be beneficial to analyze TOF spectra with a different non-uniform binning structure to maintain counting uncertainty in each bin. Studies to assess minimum detectable concentration and the assay performance versus isotope areal density and sample complexity are also warranted. These could help inform future IAEA International Target Values for assay of such samples for thorium fuel cycle safeguards.

Detector Upgrades: Acquiring, characterizing, and integrating the multi-layer BCS designed in this project and testing pNRTA performance in high radiation environments would advance the TRL of pNRTA for irradiated samples and broaden its applicability.

This page intentionally left blank.

8.0 References

Betzler, Benjamin R, William Wieselquist, and Massimilliano Fratoni. 2020. *Modeling Molten Salt Reactor Fission Product Removal with SCALE.* Oak Ridge National Lab.(ORNL), Oak Ridge, TN (United States).

Chichester, David L, and James W Sterbentz. 2012. "Assessing the feasibility of using neutron resonance transmission analysis (NRTA) for assaying plutonium in spent fuel assemblies." *Journal of Nuclear Materials Management* 40 (4): 41-52.

Compere, EL, SS Kirslis, EG Bohlmann, FF Blankenship, and WR Grimes. 1975. *Fission product behavior in the molten salt reactor experiment.* Oak Ridge National Lab.(ORNL), Oak Ridge, TN (United States).

Engel, Ezra M, Ethan A Klein, and Areg Danagoulian. 2020. "Feasibility study of a compact neutron resonance transmission analysis instrument." *AIP Advances* 10 (1): 015051. https://doi.org/https://doi.org/10.1063/1.5129961.

Evans, Louise G, Vlad Henzl, Alicia Swift, Nicholas P Luciano, Eric Cervi, Jill Cooley, Bryn Davies, Joanna S Denton, Andrea Favalli, and Brandon Grogan. 2021. *Safeguards Technology for Thorium Fuel Cycles: Research and Development Needs Assessment and Recommendations.* Oak Ridge National Lab (ORNL) (Oak Ridge, TN). https://info.ornl.gov/sites/publications/Files/Pub150423.pdf.

Fang, Ming, and Angela Di Fulvio. 2023. "Feasibility of neutron coincidence counting for spent TRISO fuel." *Annals of Nuclear Energy* 193: 110062. https://doi.org/https://doi.org/10.1016/j.anucene.2023.110062. https://www.sciencedirect.com/science/article/pii/S030645492300381X.

Guembou Shouop, Cebastien Joel, and Harufumi Tshuchiya. 2025. "Monte Carlo and experimental assessment of the optimal geometry of the source and collimator for a table-top NRTA system for small nuclear material measurement." *Nuclear Instruments and Methods in Physics Research Section A: Accelerators, Spectrometers, Detectors and Associated Equipment* 1072: 170189. https://doi.org/https://doi.org/10.1016/j.nima.2024.170189. https://www.sciencedirect.com/science/article/pii/S016890022401115X.

Heuer, D, E Merle-Lucotte, M Allibert, M Brovchenko, V Ghetta, and P Rubiolo. 2014. "Towards the thorium fuel cycle with molten salt fast reactors." *Annals of Nuclear Energy* 64: 421-429. https://doi.org/https://doi.org/10.1016/j.anucene.2013.08.002.

Houtzeel, A., and F. F. Dyer. 1972. *STUDY OF FISSION PRODUCTS IN THE MOLTEN-SALT REACTOR EXPERIMENT BY GAMMA SPECTROMETRY.* Oak Ridge National Laboratory. https://www.osti.gov/servlets/purl/4659054.

Klein, Ethan Avram. 2023. "Neutron Resonance Transmission Analysis of Nuclear Material Using a Portable D-T Neutron Generator " PhD, Department of Nuclear Science and Engineering, Massachusetts Institute of Technology. https://dspace.mit.edu/handle/1721.1/152884.

Klein, Ethan, Farheen Naqvi, Jacob Bickus, Hin Lee, Areg Danagoulian, and Robert Goldston. 2021. "Neutron-Resonance Transmission Analysis with a Compact Deuterium-Tritium Neutron

Generator." *Physical Review Applied* 15 (5): 054026. https://doi.org/10.1103/PhysRevApplied.15.054026.

Lan, Zechen, Yasunobu Arikawa, Seyed Reza Mirfayzi, Alessio Morace, Takehito Hayakawa, Hirotaka Sato, Takashi Kamiyama, Tianyun Wei, Yuta Tatsumi, Mitsuo Koizumi, Yuki Abe, Shinsuke Fujioka, Kunioki Mima, Ryosuke Kodama, and Akifumi Yogo. 2024. "Single-shot laser-driven neutron resonance spectroscopy for temperature profiling." *Nature Communications* 15 (1): 5365. https://doi.org/10.1038/s41467-024-49142-y. https://doi.org/10.1038/s41467-024-49142-y.

Lockhart, Madeline, Richard L Reed, Louise G Evans, Vlad Henzl, and John Mattingly. 2025. "Active neutron coincidence counting to determine fissile mass of uranium oxide containing 233U and 235U." *Nuclear Instruments and Methods in Physics Research Section A: Accelerators, Spectrometers, Detectors and Associated Equipment*: 170231.

Losko, Adrian Simon, and SC Vogel. 2022. "3D isotope density measurements by energy-resolved neutron imaging." *Scientific Reports* 12 (1): 1-7. https://doi.org/https://doi.org/10.1038/s41598-022-10085-3.

McDonald, B, J. Burnett, Richard A Clark, A Danagoulian, Andrew J Gilbert, E A Klein, J Kulisek, M E Moore, R. Pierson, J Rahon, G Warren, and M Zalavadia. 2022. *New NDA Methods for Thorium Fuel Cycle Safeguards: Mid-Project Report (PNNL-33726).* Pacific Northwest National Laboratory. http://www.pnnl.gov/main/publications/external/technical_reports/PNNL-33726.pdf.

McDonald, B.S., J.L. Burnett, R.A. Clark, A. Danagoulian, A.J. Gilbert, M.E. Moore, J.A. Kulisek, E.A. Klein, G.A. Warren, and M.A. Zalavadia. 2022. "NEW NDA METHODS FOR THORIUM FUEL CYCLE SAFEGUARDS " Annual Meeting of the Institute of Nuclear Materials Management.

McDonald, Benjamin S, Areg Danagoulian, Andrew J Gilbert, Ethan A Klein, Jonathan A Kulisek, Michael E Moore, Jill M Rahon, and Mital A Zalavadia. 2024. "Neutron resonance transmission analysis prototype system for thorium fuel cycle safeguards." *Nuclear Instruments and Methods in Physics Research Section A: Accelerators, Spectrometers, Detectors and Associated Equipment*: 169148. https://doi.org/https://doi.org/10.1016/j.nima.2024.169148.

REFIT-2009 A Least-Square Fitting Program for Resonance Analysis of Neutron Transmission, Capture, Fission and Scattering Data Users' Guide for REFIT-2009-10. UKNSF.

Paradela, Carlos, Jan Heyse, Stefan Kopecky, Peter Schillebeeckx, Hideo Harada, Fumito Kitatani, Mitsuo Koizumi, and Harufumi Tsuchiya. 2017. "Neutron resonance analysis for nuclear safeguards and security applications." *EPJ Web Conf.* 146: 09002. https://doi.org/10.1051/epjconf/201714609002.

Postma, H, and P Schillebeeckx. 2017. "Neutron resonance analysis." In *Neutron Methods for Archaeology and Cultural Heritage*, edited by N. Kardjilov and G. Festa, 235-283. Swizerland: Springer International Publishing.

Priesmeyer, HG, and U Harz. 1975. "Isotopic content determination in irradiated fuel by neutron transmission analysis." *Atomkernenergie* 25 (2): 109-113.

Rahon, Jill M. 2024. "Compact Capabilities: Developing and Evaluating a Field-Portable Neutron Resonance Capture Analysis System." Massachusetts Institute of Technology. https://dspace.mit.edu/handle/1721.1/157134.

Searfus, Oskar, Peter Marleau, Eva Uribe, Heather Reedy, and Igor Jovanovic. 2023. "Passive and active neutron signatures of ^{233}U for nondestructive assay." *Physical Review Applied* 20 (6): 064038.

Subzwari, S, A Danagoulian, J Rahon, and B McDonald. 2024. "Detector Mechanisms for a Portable Nuclear Resonance Transmission Analysis Device." 2024 IEEE Nuclear Science Symposium (NSS), Medical Imaging Conference (MIC) and Room Temperature Semiconductor Detector Conference (RTSD).

Subzwari, Shayaan. 2025. "Neutron Resonance Transmission Analysis of Nuclear Material for Reactor Safeguards Applications." Masters of Science, Nuclear Science and Engineering, Massachusetts Institute of Technology.

Subzwari, Shayaan, J Rahon, E Klein, B McDonald, M Zalavadia, M Moore, J Kulisek, and Areg Danagoulian. 2024. "Neutron Resonance Transmission Analysis for the Thorium Fuel Cycle & High-Gamma Emitting Targets." Institute of Nuclear Materials Management Annual Meeting. https://resources.inmm.org/annual-meeting-proceedings/neutron-resonance-transmission-analysis-thorium-fuel-cycle-high-gamma.

Taylor, L L, and H H Loo. 1999. *Shippingport LWBR (Th/U Oxide) Fuel Characteristics for Disposal Criticality Analysis.* (United States). https://www.osti.gov/biblio/769053.

Zalavadia, M. A., A. Danagoulian, E. A. Kelin, M. E. Moore, F. Naqvi, G. A. Warren, and R. S. Wittman. 2021. *Isotope Verification for Arms Control: FY21 Progress Report.* Pacific Northwest National Laboratory (Richland, WA).

Zhang, Yuxuan, Jean-C Bilheux, Hassina Z Bilheux, and Jiao YY Lin. 2019. "An interactive web-based tool to guide the preparation of neutron imaging experiments at oak ridge national laboratory." *Journal of Physics Communications* 3 (10): 103003. https://doi.org/10.1088/2399-6528/ab4ee6. https://neuit.ornl.gov/resonance.

Zhang, Yuxuan, and Jean-Christophe Bilheux. 2017. "ImagingReso: A tool for neutron resonance imaging." *Journal of Open Source Software* 2 (19).

Appendix A Project Research Products

This appendix contains a list of publications, presentations, and dissertations that resulted completely or in part via this project at the time of this report's completion. Additional publications are currently in progress.

Dissertations

1. Ethan A. Klein, "Neutron Resonance Transmission Analysis of Nuclear Material Using a Portable D-T Neutron Generator." MIT PhD Thesis, 2023. (E.A. Klein 2023).
2. Jill M. Rahon, "Compact Capabilities: Developing and Evaluating a Field-Portable Neutron Resonance Capture Analysis System." MIT PhD Thesis, 2024. (Rahon 2024).
3. Shayaan Subzwari, "Neutron Resonance Transmission Analysis of Nuclear Material for Reactor Safeguards Applications." MIT Master's Thesis, 2025. (Shayaan Subzwari 2025).

Publications

1. Benjamin S. McDonald, Areg Danagoulian, Andrew J. Gilbert, et al. "Neutron resonance transmission analysis prototype system for thorium fuel cycle safeguards." Nuclear Instruments and Methods in Physics Research, Section A. 2024. (Benjamin S McDonald et al. 2024).

Reports

1. Benjamin S. McDonald, Jonathan Burnett, Richard Clark, et al. "New NDA Methods for Thorium Fuel Cycle Safeguards." Mid-Project Report, 2022. PNNL- 33726. (B. McDonald, Burnett, Clark, Danagoulian, Gilbert, Klein, et al. 2022). URL: http://www.pnnl.gov/main/publications/external/technical_reports/PNNL-33726.pdf

Conference Presentations & Proceedings

1. Benjamin S. McDonald, et al. "New Methods for Thorium Fuel Cycle Safeguards." Proceedings of the INMM 63rd Annual Meeting, 2022. (B.S. McDonald, Burnett, Clark, Danagoulian, Gilbert, Moore, et al. 2022).

2. Benjamin S. McDonald, et al. "Demonstration of Neutron Resonance Transmission Analysis for Thorium Fuel Cycle Safeguards." Symposium on Radiation Measurements and Applications, 2023. (PNNL-SA-185300).

3. Michael E. Moore., et al. "Portable Neutron Resonance Transmission Analysis for Advanced Reactor Safeguards." Crossroads of Nonproliferation and Safeguarding Technologies for Implementation in Molten Salt Reactors, Idaho Falls, Idaho. PNNL-SA-192974, 2023.

4. Shayaan Subzwari, et. al. "Neutron Resonance Transmission Analysis for the Thorium Fuel Cycle & High-Gamma Emitting Targets." Proceedings of the INMM 65th Annual Meeting, 2024. (Shayaan Subzwari 2025).

5. Shayaan Subzwari, et al. “Detector Mechanisms for a Portable Nuclear Resonance Transmission Analysis Device.” IEEE Nuclear Science Symposium, 2024. (S Subzwari, Danagoulian, et al. 2024).

6. Presentations at 2023-2025 program reviews (NSARD, MTV Workshop, NNSA University Program Review).

Pacific Northwest National Laboratory

902 Battelle Boulevard
P.O. Box 999
Richland, WA 99354

1-888-375-PNNL (7665)

www.pnnl.gov